Thermal Infrared and Optical Observations of Four Near-Earth Asteroids

Stephen D. Wolters[a], Simon F. Green[a], Neil McBride[a], and John K. Davies[b]

[a] *Planetary and Space Sciences Research Institute, The Open University, Milton Keynes, MK7 6AA, UK*
[b] *Astronomy Technology Centre, Royal Observatory Edinburgh, Blackford Hill, Edinburgh EH9 3HJ, UK*

Submitted to ICARUS: 01 February 2007
Revised: 23 May 2007
Revised: 07 August 2007
No. of manuscript pages: 49
No. of figures: 9
No. of Tables: 4

Please direct editorial correspondence and proofs to:

Stephen Wolters
Planetary and Space Sciences Research Institute
The Open University
Walton Hall
Milton Keynes
Buckinghamshire
MK7 6AA
UK

Phone: +44 1908 659465
e-mail: s.d.wolters@open.ac.uk

e-mail addresses of co-authors: s.f.green@open.ac.uk, n.m.mcbride@open.ac.uk, and jkd@roe.ac.uk.

Abstract

We present thermal infrared photometry and spectrophotometry of four Near-Earth Asteroids (NEAs), namely (433) Eros, (66063) 1998 RO_1, (137032) 1998 UO_1, and (138258) 2000 GD_2, using the United Kingdom Infrared Telescope (UKIRT) in 2002. For two objects, i.e.: (433) Eros and (137032) 1998 UO_1 quasi-simultaneous optical observations were also obtained, using the Jacobus Kapteyn Telescope (JKT). For (127032) 1998 UO_1, we obtain a rotation period P = 3.0 ± 0.1 h and an absolute visual magnitude H_V = 16.7 ± 0.4. The Standard Thermal Model (STM), Fast Rotating Model (FRM) and Near-Earth Asteroid Thermal Model (NEATM) have been fitted to the IR fluxes to determine effective diameters D_{eff}, geometric albedos p_v, and beaming parameters η. The derived values are (433) Eros: D_{eff} = 23.3 ± 3.5 km (at lightcurve maximum), p_v = 0.24 ± 0.07, η = 0.95 ± 0.19; (66063) 1998 RO_1: $D_{eff} = 0.62^{+0.25}_{-0.09}$ km, $p_v = 0.30^{+0.09}_{-0.17}$; (137032) 1998 UO_1: D_{eff} < 1.13 km, p_v > 0.29; (138258) 2000 GD_2: D_{eff} = 0.27 ± 0.04 km, $p_v = 0.56^{+0.32}_{-0.22}$, η = 0.74 ± 0.15. (66063) 1998 RO_1 is a binary asteroid from lightcurve characteristics (Pravec *et al.*, 2006) and we estimate the effective diameter of the primary (D_p) and secondary (D_s) components: $D_p = 0.56^{+0.23}_{-0.09}$ km and $D_s = 0.27^{+0.13}_{-0.05}$ km. The diameter and albedo of (138258) 2000 GD_2 are consistent with the trend of decreasing diameter for S- and Q-type asteroids found by Delbó *et al.* (2003). A possible trend of increasing beaming parameter with diameter for small (less than about 3 km) S- and Q-type asteroids is found.

1 Introduction

1.1 Need for NEA Characterisation

A Near-Earth Asteroid (NEA) is defined as an asteroid having a perihelion distance $q \leq$ 1.3 AU and aphelion distance $Q >$ 0.983 AU. Studies of NEAs are important for understanding their origin and evolution, the links between meteorites and their parent bodies, and for assessing the impact hazard. NEAs may also be representative of small main belt asteroids (Binzel *et al.*, 2002).

The discovery rate of NEAs is vastly outstripping their physical characterisation, as described by Cellino *et al.* (2002). As of April 2007, the number of NEAs with measured diameters and albedos is about 90 (most of which can be found at http://earn.dlr.de/nea/table1_new.html) while the total number of NEAs discovered is over 4500 (http://neo.jpl.nasa.gov/). Increased measurements of the diameters and albedos of NEAs are needed for a more accurate derivation of their size distribution, which is crucial for assessment of the impact hazard and for optimising survey strategies.

Smaller NEAs below 1 km particularly need to be characterized; but unfortunately there is an observational selection bias. Prior to measuring the thermal IR flux, we are unable to distinguish between small, high-albedo and large, low-albedo objects, and so there can be a tendency to prioritise only on visible brightness, presuming that more thermal flux will be received since a brighter object is more likely to be larger. Therefore we are most likely to *try* to observe *large, high-albedo* objects, less likely small, high-albedo and large, low-albedo objects, and least likely small, low-albedo objects. The larger and lower-albedo an object is, the greater the absorbed and re-emitted thermal IR flux. So we are most likely to *succeed* in measuring IR flux from *large, low-albedo* objects, less from small, low-albedo and large, high-albedo objects, and least from small, high-albedo objects.

If a correlation between albedo and taxonomic type can be used to derive an average albedo for each type, they can be used to derive a de-biased size distribution. Stuart and Binzel (2004), making use of an extended database of spectroscopic observations, have done the first study using albedo statistics from NEAs, obtained from Delbó *et al.* (2003). However, the average values of the albedos of A, R and U-types are still obtained from main-belt statistics and several values are based on very few classified objects (for example the D-type complex had only one member with a measured albedo in this study).

1.2 Radiometric Diameter Determination

An asteroid's effective diameter [the equivalent diameter of a perfect sphere with the same projected area as the (generally) irregularly shaped asteroid] can be roughly constrained from its absolute visual magnitude H_V by assuming a range of possible geometric albedo p_v (e.g. 0.03-0.6) and following Fowler and Chillemi (1992):

$$D_{\text{eff}}\left(\text{km}\right) = \frac{10^{-H_V/5}\,1329}{\sqrt{p_v}} \tag{1}$$

For example, an asteroid with $H_V = 17.0 \pm 0.5$ could have a diameter between 0.5 and 3.9 km.

If we can measure both the scattered sunlight at an asteroid's surface and the absorbed and re-emitted thermal IR flux, a unique albedo and diameter can be derived. However we cannot directly measure the total radiation emitted in all directions. Instead a thermal model is used to simulate a surface temperature distribution. We used three simple thermal models: the Standard Thermal Model (STM, Lebofsky *et al.*, 1986), the Fast Rotating Model (FRM, e.g. Lebofsky and Spencer, 1989) and the Near-Earth Asteroid Thermal Model (NEATM, Harris, 1998). Ideally, a full thermophysical model would be used, but the necessary physical characteristics are not generally known (e.g. spin axis, shape) for

most NEAs, for which observations are often limited to short duration close approaches to the Earth. However, a growing subset of objects have had their diameters and albedos measured using a thermophysical model [e.g. Harris *et al.* (2005), Müller *et al.* (2005)].

The Planck function is numerically integrated over the visible hemisphere to provide a model IR flux $F_{mod}(\lambda_n)$, which can be best-fit to the observed fluxes $F_{obs}(\lambda_n)$. The fitted D_{eff} will be appropriate for the projected area at the time of the thermal IR observation, and not at the mean or maximum lightcurve as it is commonly presented in the literature. Therefore if a quasi-simultaneous lightcurve is available, D_{eff} can be adjusted to the mean H_V, assuming that the optical and thermal lightcurves correspond.

Neither the STM nor the FRM provide in general accurate diameters for NEAs (e.g. Veeder et al., 1989). This is because the STM models the temperature distribution for an asteroid with either thermal inertia $\Gamma = 0$ or rotation frequency $\omega = 0$ (or both), while the FRM assumes $\Gamma \rightarrow \infty$ or $\omega \rightarrow \infty$ (or both). They both give poor representations of NEA temperature distributions because these objects have intermediate thermal inertias [e.g. ~200 J m^{-2} $s^{-1/2}$ K^{-1}, (Delbo' et al., 2007)], between those of large main belt asteroids [<~50 Jm^{-2} $s^{-1/2}$ K^{-1} (Müller and Lagerros, 1998), for which the STM works fine] and that of the bare rock (~>2200 Jm-2 $s^{-1/2}$ K^{-1}). The NEATM was introduced to solve the above problem (Harris, 1998). Additionally, NEAs are often observed at high phase angle.

In the NEATM, the maximum temperature (T_{max}) is given by:

$$T_{\max} = \left[\frac{(1-A)S}{\eta \varepsilon \sigma} \right]^{\frac{1}{4}} \qquad (2)$$

where A is the bolometric Bond albedo, S is the incident solar flux, η is the so-called "beaming parameter", ε is the thermal IR emissivity [0.9 is assumed, see e.g. Lim *et al.* (2005b) and Delbo' *et al.* (2007) for discussions on the effect of changing ε], and σ is the Stefan-Boltzmann constant. NEATM models the asteroid as a sphere and calculates the temperature on the surface assuming Lambertian emission on the day side and zero emission on the night side. The NEATM allows η to be varied until $F_{mod}(\lambda_n)$ gives a best fit to the observed thermal IR spectrum $F_{obs}(\lambda_n)$, effectively forcing the model temperature distribution to show a colour temperature consistent with the apparent colour temperature implied by the data. Delbó *et al.* (2003) discovered a trend of increasing η with phase angle α, and suggested using $\eta = 1.0$ for $\alpha < 45°$ and $\eta = 1.5$ for $\alpha > 45°$ for cases where color information is unavailable. For more detailed discussion of the radiometric method of diameter determination and the NEATM see Delbó and Harris (2002), Harris and Lagerros (2002), and references therein.

Best-fitting the beaming parameter can compensate for an altered temperature distribution due to beaming. It can also compensate for, to some extent, non-zero thermal inertia and not including thermal emission on the night side. However, at phase angles $\alpha > 45°$ NEATM can become significantly inaccurate, and will overestimate the diameter by ~10%-40% and underestimate the albedo. The inaccuracy increases with α and depends on whether the morning or evening side is observed (Wolters, 2005; Wolters and Green, in preparation).

2 Observations

The observations reported in this paper complete the dataset of NEAs observed at the United Kingdom Infrared Telescope (UKIRT) and quasi-simultaneously at the Jacobus Kapteyn Telescope (JKT) in 2002 begun by Wolters *et al.* (2005).

2.1 Optical Observations

The primary goal of all September/October 2002 JKT observations was to produce optical observations to complement thermal IR observations. Ideally, enough observations would be taken to create a composite lightcurve, from which the absolute visual magnitude H_V at the midpoint of the time of the UKIRT thermal IR observations can be determined. Observations of (433) Eros were taken at the 1.0 m JKT on 28.1, 29.0 and 30.0 September 2002 UT, and of (137032) 1998 UO_1 on 26.2 September 2002 UT. Observations were taken in the V-filter with a SITe2 CCD camera with an image scale of 0.33 arcsec/pixel giving a field of view of about 10 × 10 arcmin. The observational circumstances and instrument configuration are given in Table 1. The data were obtained and reduced using the methodology described in Wolters *et al.* (2005).

2.2 Thermal IR Observations

Michelle is a mid-infrared imager/spectrometer with a SBRC Si:As 320 × 240-pixel array operating at 8-25 μm. When used in imaging mode Michelle provides a 67.2 × 50.4 arcsec field of view at 0.21 arcsec/pixel. Thermal IR photometry was taken of (138258) 2000 GD_2 at the UKIRT on 23 March 2002 UT under clear skies, using the Michelle instrument in imaging mode at 10.3, 12.5 and 18.5 μm. Determination of the extinction and photometric calibration was done using stars BS 4728 and BS 3748. Absolutely calibrated N- and Q-band magnitudes for standard stars were obtained from Tokunaga (1984) and Rieke *et al.* (1985). The observations were obtained and reduced using the methodology described in Wolters *et al.* (2005).

Thermal IR spectrophotometry was taken of (433) Eros, (66063) 1998 RO_1 and (137032) 1998 UO_1 in September 2002 UT using the Michelle instrument in spectroscopy

mode, in which it has a resolution of 0.38 arcsec/pixel. The observations were taken using the lowN grating covering 7-12.5 μm, and calibration was performed using bias frames, flat fields, standard and ratio stars as described in Wolters *et al.* (2005).

Where ratio stars' magnitudes were independently measured on different nights, the difference in magnitude can provide an estimate of the typical uncertainty in absolute flux calibration. We adopt a 7% uncertainty from this source of error. However, the uncertainties in our asteroid diameter determinations are dominated by thermal-model dependent uncertainties. In general for our targets in September 2002 we used 4 pixels slit width to ensure acquiring the same percentage flux in both the standard stars and the targets for absolute flux calibration. However, on 29 September, due to concerns about cirrus, we used 2 pixel slits to prevent possible background saturation. Our experience suggests that we obtained good absolute flux calibration on 29 September, despite only using a 2 pixel slit, since objects observed on both 29 September (in the early night when cirrus was not apparent) and other nights using a 4 pixel slit, had the same flux levels and derived diameters: 2000 ED_{104} and 2002 NX_{18} in Wolters *et al.* (2005). Nevertheless, for 1998 RO_1 we introduce a factor of 2 into our assumptions for the flux uncertainty as described in Section 2.2.1.

The observational circumstances and instrument configuration are given in Table 1. Notes on individual objects are given below.

2.2.1 (66063) 1998 RO_1

(66063) 1998 RO_1 is the only asteroid with a flux-calibrated asteroid spectrum observed on 29 September, where there was intermittent cirrus, that was not observed on other nights. The uncertainty in the fluxes must therefore be increased. We can estimate how much the flux could be underestimated by calculating the average difference in N-

band fluxes for asteroids that were observed on 29 September and also on other nights (described in Wolters *et al.*, 2005), which we calculate as a factor of 2. The uncertainty in the thermal model fits to the (66063) 1998 RO_1 fluxes must take this flux underestimation into account.

2.2.2 (137032) 1998 UO_1

There is a little understood source of noise in the Michelle detector array which we refer to as 'electronic pickup' that, out of the objects reported here, only significantly affected (137032) 1998 UO_1. Before charge accumulation begins, each pixel is reset to some initial value. Because of thermal noise it is not possible to know precisely what this initial value is from one reset operation to the next. This would introduce a fundamental uncertainty in the total charge measured if each pixel was only read once at the end of the integration period. To avoid this, Michelle performs doubly-correlated sampling, in which the array is read shortly after reset (non-destructively) and then again at the end of a specified integration period. The difference between the two readouts gives the desired counts per integration period and to lower the effect of readout noise the chip can be read several times. Averaging the successive differences reduces the effective readout noise. When the exposure time is reduced to 0.1 s or less, Michelle is no longer able to use non-destructive reads. It may be that that this is the cause of the electronic pickup noise. The noise is only significant in frames taken using the wider (4-pixel) slit width, where the exposure time is reduced to 0.1 s automatically in order to avoid saturating the array. When the 2-pixel slit was used on 29 September, as for (66063) 1998 RO_1, the noise is negligible. (433) Eros is bright enough that the contribution of electronic pickup is also negligible. However, for our faintest object (137032) 1998 UO_1 the noise completely masked the signal.

No spectrum was found to be extracted from the (137032) 1998 UO_1 group file. Since the asteroid spectrum was not clearly seen, a 3 pixel diameter optimum extraction was performed on the same rows as the spectrum was extracted from the accompanying ratio star. Limits on the maximum D_{eff} and minimum p_v can be estimated from the amplitude of the noise. Since the noise is dominated by electronic pickup, we optimally extracted a spectrum using row centres -8 to +8 pixels around the same row centres used to extract the ratio star. The resulting variation in N-band flux is seen in Fig. 1. The amplitude of the variation in flux due to this noise is found to be 3.4×10^{-15} W m^{-2} μm^{-1}. This noise estimate will be used to estimate D_{eff} and p_v limits in Section 4.3.

3 Results and Data Analysis from Optical Observations

3.1 (433) Eros

(433) Eros is one of the largest and probably the most studied NEA, particularly after the NEAR Shoemaker spacecraft orbited it from 14 February 2000, eventually landing on the asteroid on 12 February 2001 (Cheng, 2002). A good overview on what the NEAR Shoemaker mission has discovered about Eros can be found in Sullivan *et al.* (2002). Eros is an S-type asteroid; we follow the taxonomic classification scheme of Bus and Binzel (2002) throughout. It has a rotation period of 5.270 h and its lightcurve amplitude can range from 0.04-1.49 mag. depending on viewing geometry (e.g. Campa, 1938). Its absolute magnitude is $H_V = 10.30 \pm 0.05$ (Erikson *et al.*, 2000). A triaxial ellipsoid fit to the more complex elongated shape of 34.4 × 11.2 × 11.2 km is found from the Multispectral Imager (Veverka *et al.*, 2000), in good agreement with previous lightcurve and radar studies [Zellner (1976), Mitchell *et al.* (1998)]. As part of the NEAR Radio Science investigation, Konopliv *et al.* (2002) found a highly accurate spin state solution of:

rotation period P = 5.27025527 ± 0.00000003 h, pole right ascension and declination α = 11.363 ± 0.001°, δ = 17.232 ± 0.001° (J2000).

The 28.1, 29.0 and 30.0 September reduced magnitude lightcurve was Fourier fitted with a 6th order solution (Fig. 2). The derived best-fit synodic rotation period solution was P = 5.249 ± 0.001 h. The maximum difference ΔP between the synodic period P_{syn} (the time it takes Eros to complete one revolution relative to the Earth) and the sidereal period P_{sid} (the time to complete one revolution relative to the stars) is given by (Pravec *et al.*, 1996):

$$\Delta P = \pm \omega_{PAB} P_{syn}^2 \tag{3}$$

where ω_{PAB} is the angular velocity of the phase angle bisector (PAB) (± depending on rotation direction). If one bisected the angle formed by the lines to the Sun and the Earth from the asteroid, the resultant line would be in the direction of the PAB. The PAB changed from longitude L_{PAB} = 351.0462° and latitude B_{PAB} = 15.3555° to L_{PAB} = 351.0467° and B_{PAB} = 15.3581°. This gives ω_{PAB} = 1.5 ×10^{-5} rad./h. We arrive at the result ΔP = 0.0004h, so the difference between our measured value of P_{syn} = 5.249 h and the true value of P_{sid} = 5.270 h, about 1.5 min., cannot be accounted for by this effect. This gave us a rough idea of the real uncertainty of our period measurements, which is larger than the formal uncertainty we quote that results from the residuals in the Fourier fitting. Since the main purpose of observing (433) Eros was to test our methods, including lightcurve correction, for deriving diameters and albedos of NEAs from thermal IR observations, we used the P = 5.249 h solution for lightcurve correction.

The 28.1 September observations were judged to be photometric, and the fitted magnitudes of the other nights were adjusted to this night. The final uncertainty of the derived mean visual magnitude $\overline{V}(\alpha)$ is obtained from the uncertainty of the apparent magnitude of the comparison star, which is based on the (negligible) standard error of the

derived value (± 0.003 mag.), the Fourier fitting uncertainty given in the caption of Fig. 2, and the estimated atmospheric extinction correction uncertainty (± 0.04 mag.). Thus we obtain $\overline{V}(\alpha = 18.0°)$ = 11.28 ± 0.04. Applying G = 0.146 for (433) Eros (Domingue *et al.*, 2002) gives H_V = 10.34 ± 0.04 (the uncertainty assumes no inaccuracy in G). This is in agreement with Erikson *et al.* (2000).

We can define the lightcurve amplitude from the second harmonic of the Fourier fit to the composite lightcurve (Pravec *et al.*, 1996), which we refer to as the "peak-to-valley" amplitude A_{fit}.

$$A_{fit} = 2\sqrt{C_2^2 + S_2^2} \tag{4}$$

where C_2 and S_2 are the second order Fourier coefficients. We can also define a "manually" measured amplitude A_{man} of the observed lightcurve extrema which allows comparison with data given by other researchers.

The measured lightcurve amplitude depends on the phase angle of observation. This is known as the amplitude-phase effect. Zappalà *et al.* (1990) analysed the amplitude phase relation (APR) using geometrical and laboratory models and a real asteroid dataset. They found that the slope m of the APR turns out to be a function of the amplitude at 0° phase angle $A(0°)$ only:

$$A(0°) = A(\alpha)/(1 + m\alpha) \tag{5}$$

From the asteroid dataset, they determined that for a general asteroid m = 0.018. They were able to determine values of m for different taxonomic types and found m(S) = 0.030. However, the assumption of a linear APR is only valid for α < 40°, and for larger values one can overestimate the actual amplitude at 0°. However, previous authors have applied this correction to NEAs observed at high phase angles (e.g. Binzel *et al.*, 2002), and we will apply the same correction to the amplitude measured for (137032) 1998 UO_1 (Section 3.2).

For (433) Eros we measure $A_{fit}(\alpha=18°) = 0.06$ mag. and $A_{man}(18°) = 0.10$ mag. This is at the lower end of the range of measured lightcurve amplitudes for Eros. Comparing the spin axis RA and DEC from Konopliv *et al.* (2002) with Eros' latitude and longitude (L =344.797° and B = 22.037°) shows that the asteroid is nearly pole-on, so we should expect a small lightcurve amplitude. Adopting A_{man}, we find $A(0°) = 0.06$ mag, using $m = 0.030$ in Eq. 5.

The midpoint of the 28 September 2002 UT UKIRT observation was at rotational phase 0.59 (t_0 = 0h 25 September 2002 UT), and so an absolute visual magnitude H_V = 10.32 was used for the thermal IR fitting.

3.2 (137032) 1998 UO_1

Pravec and colleagues have observed (137032) 1998 UO_1 in October 2004 (www.asu.cas.cz/~ppravec/neo.htm) and found P = 2.90 ± 0.02 h and a low lightcurve amplitude 0.04 mag. Our reduced magnitudes for the 26.2 September 2002 UT JKT observations only just cover a long enough period of time (3.2 h) to encompass the entire lightcurve. A 4th order Fourier best-fit gives a period of P = 3.033 ± 0.006 h (Fig. 3). However, we can see that only two observations taken at the beginning (white squares) overlap in rotational phase with observations taken at the end (white triangles) so the period we obtain is dependent on how we mesh these few points. We therefore assign a larger uncertainty to the period to account for the possible freedom in adjusting the overlap of these points: P = 3.0 ± 0.1 h. This period is consistent with that found by Pravec. We derive $\overline{V}(\alpha = 47.2°)$ = 18.51 ± 0.04. Assuming $G = 0.15^{+0.25}_{-0.15}$, this corresponds to H_V = 16.7 ± 0.4. We obtain lightcurve amplitudes A_{fit} = 0.1 and A_{man} = 0.16.

The amplitude can be used to constrain the asteroid's shape. If we assume the asteroid is a triaxial ellipsoid with axes a, b and c ($a \geq b \geq c$) rotating about the c axis (the most

dynamically stable solution, and so typically a good approximation) the lightcurve amplitude may be given by (Binzel *et al.*, 1989):

$$A(\theta) = 2.5\log\left(\frac{a}{b}\right) - 1.25\log\left(\frac{a^2\cos^2\theta + c^2\sin^2\theta}{b^2\cos^2\theta + c^2\sin^2\theta}\right) \quad (6)$$

where θ is the aspect angle (the angle between observer's line of sight and asteroid spin vector). If an asteroid is viewed at an equatorial aspect, then the second term in Eq. 6 is zero and the lightcurve would have its maximum possible amplitude as the projected surface area changes from πac to πbc. If an asteroid is viewed pole-on, then no change in projected surface area is seen and the expected amplitude is zero. Hence, if we have no information on θ at all we can assume it is equatorial to define the minimum ratio between a and b:

$$\frac{a}{b} > 10^{0.4A} \quad (7)$$

Adopting A_{man} and correcting to zero degree phase angle gives $A(0°) = 0.09$, corresponding to minimum $a/b = 1.08$.

The midpoint of the 28 September 2002 UT UKIRT observation was at rotational phase 0.38 (t_0 = 0h 25 September 2002 UT), and so an absolute visual magnitude H_V = 16.66 was used for the thermal IR fitting.

4 Results and Data Analysis from Thermal IR Observations

The STM, FRM, and NEATM, using both a default beaming parameter η and a best-fit η, are best-fitted to the thermal IR fluxes using the method described in Section 1.2 to derive effective diameters D_{eff}, geometric visual albedos p_v and beaming parameter η. The thermal IR fluxes are given in Table 2, and the derived values are given in Table 3. For (137032) 1998 UO_1, only the NEATM was fitted to derive limits.

The uncertainty resulting from the application of the thermal model, for example due to disregarding the night side thermal flux, typically dominates over the uncertainty in the flux calibration and the scatter due to atmospheric absorption, as assessed in Wolters *et al.* (2005). Delbo (2004) and Harris (2006) have shown that the relative uncertainty in the diameter determination of the NEATM is <15% for phase angles <45°. For (66063) 1998 RO_1 the uncertainty is even greater due to the possible cirrus during the observation. For this asteroid, the uncertainty in the adopted result is calculated from the change in the albedo and diameter resulting from possible underestimation of the calibrated fluxes, combined in quadrature with the model fitting uncertainty.

4.1 (433) Eros

We observed (433) Eros in order to test the accuracy of Michelle thermal IR measurements by comparing derived D_{eff}, p_v and η with those obtained by previous groundbased measurements and by the NEAR Shoemaker spacecraft. Although the diameter and albedo of (433) Eros are well known, there is some benefit to additional thermal IR observations, since they allow the reproducibility of values measured to be judged. This is particularly true of the beaming parameter η, for which few objects have had several measurements, and its uncertainty is generally given as 20% based on its reproducibility (e.g. Delbó *et al.*, 2003). Delbo' *et al.* (2007) have estimated the mean surface thermal inertia of NEAs based on a statistical inversion analysis that relies heavily on an assessment of the uncertainty of η.

Figure 4 shows the thermal model fits to (433) Eros. The NEATM fit gives $\eta = 0.95 \pm 0.19$. Our optical and thermal infrared observations were made almost pole-on (Section 3.1), hence the low lightcurve amplitude (Fig. 2). As a result, our optical observations produced a composite lightcurve with a mean $H_V = 10.34$, which is almost at lightcurve

maximum, and we derive a diameter D_{eff} = 23.3 ± 3.5 km which is similar to Harris and Davies (1999) who also observed Eros at lightcurve maximum (Table 4). Lim *et al.* (2005b), using the STM with η-fitting and an assumed Bond albedo A = 0.18, derived a diameter of D_{eff} = 21 ± 1 km from Palomar 8-13 micron spectra taken just a week previous to ours (21-22 September 2002) and η = 0.73 ± 0.07. We have applied the NEATM to the Lim *et al.* data (using H_V extrapolated from our optical observations) and derived p_v = 0.31 ± 0.09, D_{eff} = 20.2 ± 3.0 km, and η = 0.81 ± 0.16, averaging the three spectra taken over both nights. The derived D_{eff} and η are consistent within the uncertainties of those derived by Lim *et al.*

We derived an albedo p_v = 0.24 ± 0.07 for our UKIRT data, which is most consistent with the photometric model constructed of (433) Eros from NEAR-Shoemaker MSI images reported in Li *et al.* (2004) that derived p_v = 0.23. The uncertainties also bracket the albedo derived by the earlier model reported in Domingue *et al.* (2002), p_v = 0.29 ± 0.02. The three previous measured values of η are given in Table 4. The average including ours reported here is η = 0.97 and the standard deviation is 0.12, so for this object the uncertainty of η is much less than 20%. (433) Eros was nearly pole-on during our observations (sub-Solar latitude -90° and sub-Earth latitude -82.2°, JPL Horizons website) and also during the observations of Lim *et al.* (2005) (sub-Solar latitude -88° and sub-Earth latitude -84°). Observations by Lebofsky and Rieke (1979) were more equatorial (sub-Solar latitude +40° and sub-Earth latitude +18°), but observations by Harris and Davies (1999) were also pole-on (sub-Solar latitude +84° and sub-Earth latitude +86°). Since Harris and Davies (1999) were pole-on, yet measured a higher η, we cannot say whether the lower η-values measured by Lim et al. (2005) and in this work are due to the pole orientation of Eros.

4.2 (66063) 1998 RO_1

Aten asteroid (66063) 1998 RO_1 has been observed by Pravec *et al.* (2006) on each September from 2002 to 2004 and found to be a binary asteroid based on lightcurve characteristics, with a rotation period of the primary P = 2.492 h with the secondary orbiting the primary in 14.5 h. A lightcurve amplitude of 0.13-0.16 mag. was also observed, suggesting the primary is nearly spherical, while observations suggested that the secondary is an elongated body. A mean absolute visual magnitude of $H_V = 18.0 \pm 0.1$ was found by Pravec *et al.*, which we used for the thermal IR fitting since we were unable to take optical observations of this object ourselves. Pravec *et al.* found the ratio of the diameter of the secondary (D_s) to the primary (D_p) to be $D_s/D_p = 0.48 \pm 0.03$ based on an occultation event in September 2002. (66063) 1998 RO_1 was also detected with radar at Aricebo in 2003 and 2004 (L. Benner, personal communication, 2007), and the diameter of the primary was measured to be $D_p = 0.80 \pm 0.15$ km.

The NEATM best-fit η = 5.91 is physically unlikely and probably due to cirrus affecting the shape of the spectrum. Delbo (2004) showed that no combination of surface roughness, thermal inertia, or rotation period will result in η = 5.9 at any phase angle (for spherical objects). However, we can see that the FRM is a better fit than NEATM with default η = 1 (Fig. 5), suggesting that this asteroid has high surface thermal inertia. We will therefore adopt the FRM estimate of $D_{eff} = 0.62^{+0.25}_{-0.09}$ km and $p_v = 0.30^{+0.09}_{-0.17}$. If the combined observed surface area of the binary system is equal to that of a disc of diameter D_{eff} then $D_P^2 + D_S^2 = D_{eff}^2$ if both components have the same albedo. From these assumptions, we derive $D_p = 0.56^{+0.23}_{-0.09}$ km and $D_s = 0.27^{+0.13}_{-0.05}$ km. The diameter of the primary is somewhat smaller than that derived from radar data but agrees within the uncertainties.

4.3 (137032) 1998 UO_1

An estimate of the electronic pickup noise (Section 2.2.2) is the amplitude of the N-band flux from the displaced optimum row extraction centres seen in Fig. 1. This can be put into the thermal models to give limits of p_v and D_{eff} (i.e. a single binned flux of 3.4×10^{-15} W m^{-2} μm^{-1} at 10.47 μm). Using the output of NEATM with default η = 1.0, and using H_V = 16.66 ± 0.4 we obtain $p_v > 0.29$ and $D_{eff} < 1.15$ km. At the mean visual magnitude H_V = 16.70 ± 0.4 we obtain $D_{eff} < 1.13$ km. From the limit on p_v, (137032) 1998 UO_1 is not a low albedo asteroid, and unlikely to have taxonomic classes B, C, D or P.

4.4 (138258) 2000 GD_2

(138258) 2000 GD_2 is an Sq-type asteroid (Binzel *et al.*, 2004). Figure 6 shows the thermal model fits to the 23 March 2002 UT Michelle imaging mode data. The STM is an excellent fit and accordingly the best-fit η = 0.74. Unfortunately no optical observations of (138258) 2000 GD_2 are available. Therefore H_V = 19.1 from the Minor Planet Center (http://cfa-www.harvard.edu/iau/mpc.html) was used. These values are based on very few observations with imprecise calibration, and the uncertainty can be as much as ± 0.5 mag. (Pravec, personal communication, 2003). The uncertainty has negligible effect on the derived diameter, but dominates the uncertainty on the albedo. Therefore we found the best-fit p_v for H_V = 19.6 and 18.6 also to assess the uncertainty in p_v. The adopted results are $p_v = 0.56^{+0.32}_{-0.22}$ and D_{eff} = 0.27 ± 0.04 km, making (138258) 2000 GD_2 the smallest asteroid we observed. The nominal derived albedo is the highest albedo measured for an S-type NEA, to date. This result is placed in context in Section 5.

5 Discussion

5.1 Integration with Previous NEATM Fits to Thermal IR Fluxes

Table 4 shows all previously derived effective diameters D_{eff}, geometric albedos p_v, and beaming parameters, as well as those in this work, for the following (overlapping) subsets of NEAs: S-, Q-types and those with measured beaming parameters η. Some datasets were observations of a broadband *N* magnitude, or at only one or two wavelengths, and so for these objects the NEATM was used with default beaming parameter η. For early NEATM fits, $\eta = 1.2$ was used (at all phase angles α) as suggested by Harris (1998). After Delbó *et al.* (2003), $\eta = 1.0$ for $\alpha < 45°$ and $\eta = 1.5$ for $\alpha \geq 45°$ was adopted, as a result of the linear trend found of increasing η with α. Delbo (2004) included more objects producing a database with 23 objects with measured η and 39 separate observations with measurements of η in total. Figure 7 shows the trend of increasing η with α updating the dataset to include data from Wolters *et al.* (2005) and this work, data for (10302) 1989 ML (Mueller *et al.*, 2007b), and also updated values for (33342) 1998 WT_{24} and (1580) Betulia, bringing the total to 31 objects and the number of separate data points to 54. We obtain $\eta = (0.013 \pm 0.004)\alpha + (0.89 \pm 0.17)$, which is consistent with Delbo (2004)

Delbó *et al.* (2003) and Delbo (2004) found a possible trend of increasing albedo with decreasing diameter for S-type NEAs, and interpreted it as evidence for space weathering, with younger, fresher surfaces having higher albedos (although they could not exclude the possibility that this trend was the result of an observational selection effect). This is part of a pattern of evidence that indicates that Q-type asteroids [with spectra similar to ordinary chondrite meteorites, e.g. McFadden *et al.* (1984), Bus *et al.* (2002)] are converted to S-types through the process of space weathering (e.g. Clark *et al.*, 2002). Harris (2006) confirmed this trend and included Q-types, which we will do also. Harris found a lower significance trend for non-S- and Q-type asteroids as

well, and interpreted this as indicating that there is a possible influence of a detection bias against small, dark objects.

We update the dataset here and the complete list of sources for the data we used is given in Table 4. The differences between our dataset and that of Harris (2006) are: (i) two more objects added, Q-type 2002 NY_{40} (Müller *et al.*, 2004) and (138258) 2000 GD_2 reported here; (ii) (25143) Itokawa and (433) Eros p_v and D_{eff} are derived from spacecraft measurements as opposed to thermal IR fluxes, in the manner described in Table 4; (iii) mean lightcurve amplitude D_{eff} for (433) Eros and (1980) Tezcatlipoca are used, as opposed to the maximum lightcurve amplitude, to make it consistent with the other points. We determined a linear Pearson's correlation coefficient r = -0.75 (for log p_v vs. log D_{eff}), with a probability that r = 0 (i.e. the probability that there is no trend, calculated by performing a t-test) of $p < 0.001$ (Fig. 8). This does not rule out the possibility that this trend results from the inherent observational bias against detection of small low-albedo objects.

(138258) 2000 GD_2 has the highest albedo ($p_v = 0.56^{+0.32}_{-0.22}$) derived for an S-type NEA[1]. However, the uncertainty in the albedo is still large and underlines the importance of obtaining simultaneous optical observations.

5.2 The Beaming Parameter

The trend of increasing η with α has a physical explanation. NEATM allows the beaming parameter to be adjusted to fit the apparent colour temperature implied by the spectra. At low phase angles, for large main-belt asteroids with a low thermal inertia, typically covered with a mature dusty regolith, the beaming parameter will be <1 as there

[1] With the following exception: Harris (1998) measured p_v = 0.63 for (6489) Golevka based on a single broadband *N* mag. from Mottola *et al*. (1997) and using a default η = 1.2, an inappropriate value for the phase angle α = 89°; subsequent observations by Mueller *et al.* (2003) found p_v = 0.39.

is enhanced emission in the sunward direction due to surface roughness. Hence the STM gives good fits with $\eta = 0.756$ (Lebofsky *et al.*, 1986). At mid to high phase angles, the beaming parameter will be higher: for energy to be conserved, the apparent colour temperature must be lower because there is "missing" thermal flux being sent in the sunward direction.

An object with high thermal inertia will have a higher η value than an otherwise similar object with low thermal inertia, as the temperature distribution is smoothed around the body of the asteroid due to a combination of thermal lag and rotation. In this case, the increase of η is due to a difference in the temperature profile of the asteroid: the maximum temperature is lower, and there is more flux at longer wavelengths due to the cooler asteroid surface. The NEATM finds the best-fit η based on the observations, irrespective of whether η is a result of significant thermal inertia, phase angle dependent beaming, or both. One interpretation of the fact that many NEAs appear to have a value of $\eta > 1$ is that beaming due to roughness may be less than that of other solar system bodies. Another is that, due to high thermal inertia and/or fast rotation rates, the temperature distributions around the body are smoothed and there is significant thermal emission on the night side.

Delbó *et al.* (2003) assigned a conservative estimate of 20% for η, based on its reproducibility in all cases where the NEATM has been used more than once on the same object (observed on different nights and with different instrument setups). Unfortunately, this has only be done for a few objects, hence η values may be typically more reliable than this (e.g. ~10% for Eros, Section 4.1), but the statistics are not yet good enough to make a statement either way. Additionally, this naturally incorporates some variation due to differing geometry (phase angle pole orientation, heliocentric distance) of the asteroid when it was observed. There is some detailed consideration of the theoretical variation of η due to both various surface properties and changing geometry in Delbo' *et al.* (2007) using

thermophysical models. Apart from thermal inertia, most variables would cause changes in η often within the 20% uncertainty. For example, Delbo' found that a ±100% alteration in macroscopic surface roughness (which ranges from a completely smooth surface to one saturated by hemispherical craters) could cause a change in η inside the 20% uncertainty. Hence, it is worth bearing in mind as we examine the empirical variation of η with different variables in this Section, that the uncertainty assigned to η of 20%, reflected in error bars, may be over-conservative.

Higher thermal inertia and faster rotation should cause η to increase. To check if a trend is apparent, a graph of η versus rotation period P was produced [Fig. 9 (a)]. No trend is found, which is unsurprising since any effect could be masked by variations of η with phase angle (although no trend is seen if we separate observations taken at phase angles <45°) and with thermal inertia. We also checked for a trend with D_{eff} [Fig. 9 (b) and (c)] since it is conceivable that smaller diameter asteroids might retain less regolith and hence, on average, have higher surface thermal inertia. Indeed, Delbo' *et al.* (2007) has found a trend of increasing surface thermal inertia with smaller diameters, for those NEAs whose thermal inertia has been measured using thermophysical models. No trend is apparent in Fig. 9 (b) or (c).

These graphs were also produced for just the S- and Q-type NEAs. No trend was found with rotation period or with effective diameter plotted over all size ranges [Fig. 9 (d)]. Figure 9 (e) shows η versus diameter for S- and Q-type NEAs below 2.3 km (chosen because there is a large gap between 2.3 and 3.5 km, and at >3.5 km there is clearly no trend), with a least-squares-fitted trend line, both with and without 1999 NC_{43}. This asteroid was identified as anomalous by Delbó *et al.* (2003) and Wolters *et al.* (2005) based on it having an unusually large beaming parameter in α-η plots. We can see that there is a possible trend in both cases, with a Pearson's correlation coefficient [r = 0.91,

$p(r=0) = 0.013$] with 1999 NC_{43}, and [$r = 0.93$, $p(r=0) = 0.023$] without 1999 NC_{43}. However, we note that despite the strong correlation, the uncertainties in the data are large. Therefore there is a possible trend of increasing η with diameter for S and Q-type asteroids below ~3 km diameter. This trend, if real, is unexpected. If smaller diameter NEAs had higher surface thermal inertia then we might expect decreasing η with diameter. One possible explanation for this trend is that, for observations at higher phase angles, the NEATM overestimates diameters (significantly at approximately $\alpha > 45°$; Wolters, 2005; Wolters and Green, in preparation), while η also increases with phase angle. However, in Fig. 9 (e) only one object was observed at $\alpha > 45°$. We also plotted p_v versus η for S- and Q-type asteroids [Fig. 9 (f) and (g)], and there may be a possible trend of decreasing η with increasing p_v for asteroids below ~3 km diameter although the significance of the correlation is much weaker: we determined $r = -0.76$ and $p(r=0) = 0.077$.

It may be significant that the possible trend of increasing beaming parameter with diameter is only apparent for S- and Q-type NEAs. It is possible that this trend is related in some way to the trend of decreasing albedo for increasing diameters for S- and Q-type NEAs (Fig. 8) interpreted as evidence for space weathering. Smaller NEAs are thought to have younger surfaces [i.e. the time since they were catastrophically disrupted from their parent body is shorter than for larger bodies (see Davis et al., 2002)]. Perhaps something about the process of space weathering [one theory is sputtering of iron-bearing silicates by the impact of the solar wind, cosmic rays and possibly micrometeorite impacts, producing nanophase iron (e.g. Clark et al., 2002)] is changing the asteroid's surface in such a way as to increase the beaming parameter, possibly by decreasing the surface roughness on physical scales that are important for thermal IR beaming. Even though microscopic roughness, at the scale of mm and below, influences an asteroid's thermal infrared radiation, it has always been assumed that infrared beaming essentially is due to

macroscopic roughness (e.g. Lagerros, 1998 and references therein), i.e. a distribution of surface slopes or craters at scales of some cm or meters. If further observations show this trend to be real, then this contradiction must be resolved or another physical explanation for the trend must be found.

6 Conclusions

For (137032) 1998 UO_1, we obtain a rotation period $P = 3.0 \pm 0.1$ h and an absolute visual magnitude $H_V = 16.7 \pm 0.4$ from optical observations. The STM, FRM and NEATM have been fitted to thermal IR fluxes to measure geometric visual albedos p_v, effective diameters D_{eff} and beaming parameters η. The derived values are (433) Eros: $p_v = 0.24 \pm 0.07$, $D_{eff} = 23.3 \pm 3.5$ km (at lightcurve maximum), $\eta = 0.95 \pm 0.19$; (66063) 1998 RO_1: $p_v = 0.30^{+0.09}_{-0.17}$, $D_{eff} = 0.62^{+0.25}_{-0.09}$ km; (137032) 1998 UO_1: $p_v > 0.29$, $D_{eff} < 1.13$ km; (138258) 2000 GD_2: $p_v = 0.56^{+0.32}_{-0.22}$, $D_{eff} = 0.27 \pm 0.04$ km, $\eta = 0.74 \pm 0.15$. If we assume both components have the same albedo, then the effective diameter of the primary (D_p) and secondary (D_s) components of binary asteroid (66063) 1998 RO_1 can be determined from a measurement of D_s/D_p in Pravec *et al.* (2006), and are: $D_p = 0.56^{+0.23}_{-0.09}$ km and $D_s = 0.27^{+0.13}_{-0.05}$ km. The nominal albedo of S-type (138258) 2000 GD_2 is one of the highest measured for an NEA and is consistent with the trend of increasing albedo with decreasing diameter for S- and Q-type asteroids. There is a possible trend of increasing beaming parameter with diameter for S- and Q-type asteroids below about 3 km.

Acknowledgements

The Jacobus Kapteyn Telescope was operated on the island of La Palma by the Royal Greenwich Observatory in the Spanish Observatorio del Roque de los Muchachos of the Instituto de Astrofisica de Canarias. The United Kingdom Infrared Telescope is operated

by the Joint Astronomy Centre on behalf of the U.K. Science and Technology Facilities Council (STFC). We thank: the UKIRT Telescope Operators T. Wold and W. Varricatt; referees M. Delbo' and L. Lim for helpful and incisive reviews; T. Kerr and P. Hirst for their invaluable troubleshooting of ORAC-DR; P. Pravec and L. Benner for information and advice on (66063) 1998 RO_1. We are grateful to A. Fitzsimmons for some ideas on beaming parameter trends. The work of S. D. Wolters was supported by the U.K. Particle Physics and Astronomy Research Council (PPARC, now STFC).

References

Binzel, R. P., Farinella, P., Zappalà, V. and Cellino, A. 1989. Asteroid Rotation Rates: Distributions and Statistics. In: R. P. Binzel, T. Gehrels and M. S. Matthews (Eds.), Asteroids II, University of Arizona Press, Tucson, pp. 416-441.

Binzel, R. P., Lupishko, D. F., Di Martino, M., Whiteley, R. J. and Hahn, G. J. 2002. Physical properties of near-Earth objects. In: W. F. Bottke, A. Cellino, P. Paolicchi and R. P. Binzel (Eds.), Asteroids III, University of Arizona Press, Tucson, pp. 251-271.

Binzel, R. P., Rivkin, A. S., Stuart, J. S., Harris, A. W., Bus, S. J. and Burbine, T. H. 2004. Observed spectral properties of near-Earth objects: results for population distribution, source regions, and space weathering processes. Icarus 170, 259-294.

Bus, S. J. and Binzel, R. P. 2002. Phase II of the Small Main-Belt Asteroid Spectroscopic Survey. Icarus 158, 146-177.

Bus, S. J., Vilas, F. and Barucci, M. A. 2002. Visible-wavelength spectroscopy of asteroids. In: W. F. Bottke, A. Cellino, P. Paolicchi and R. P. Binzel (Eds.), Asteroids III, The University of Arizona Press, Tucson, pp. 169-182.

Campa, M. 1938. Rotation Period of 433 Eros. Mem. Soc. Astron. Ital. 11, 285-301.

Cellino, A., Zappalà, V. and Tedesco, E. F. 2002. Near-Earth objects: origins and need of physical characterization. Meteorit. Planet. Sci. 37, 1965-1974.

Cheng, A. F. 2002. Near Earth Asteroid Rendezvous: Mission Summary. In: W. F. Bottke, A. Cellino, P. Paolicchi and R. P. Binzel (Eds.), Asteroids III, The University of Arizona Press, Tucson, pp. 351-366.

Clark, B. E., Hapke, B., Pieters, C. and Britt, D. 2002. Asteroid space weathering and regolith evolution. In: W. F. Bottke, A. Cellino, P. Paolicchi and R. P. Binzel (Eds.), Asteroids III, The University of Arizona Press, Tucson, pp. 585-599.

Davis, D. R., Durda, D. D., Marzari, F., Campo Bagatin, A. and Gil-Hutton, R. 2002. Collisional Evolution of Small-Body Populations. In: W. F. Bottke, A. Cellino, P. Paolicchi and R. P. Binzel (Eds.), Asteroids III, The University of Arizona Press, Tucson, pp. 545-558.

Delbo', M., dell'Oro, A., Harris, A. W., Mottola, S. and Mueller, M. 2007. Thermal inertia of near-Earth asteroids and implications for the magnitude of the Yarkovsky effect. Icarus In Press.

Delbo, M. 2004. The nature of near-Earth asteroids from the study of their thermal infrared emission. PhD thesis, Freie Universität, Berlin.

Delbó, M. and Harris, A. W. 2002. Physical properties of near-Earth asteroids from thermal infrared observations and thermal modeling. Meteoritics and Planetary Science 37, 1929-1936.

Delbó, M., Harris, A. W., Binzel, R. P., Pravec, P. and Davies, J. K. 2003. Keck observations of near-Earth asteroids in the thermal infrared. Icarus 166, 116-130.

Domingue, D. L., Robinson, M., Carcich, B., Joseph, J., Thomas, P. and Clark, B. E. 2002. Disk-integrated photometry of 433 Eros. Icarus 155, 205-219.

Erikson, A., Mottola, S., Lagerros, J. S. V., Lindgren, M., Piironen, J., Oja, T., Hahn, G., Lagerkvist, C.-I., Harris, A. W., Nathues, A. and Neukem, G. 2000. The Near-Earth Object Follow-up Program. Icarus 147, 487-497.

Fowler, J. W. and Chillemi, J. R. 1992. IRAS asteroid data processing. In: (Eds.), The IRAS Minor Planet Survey, Phillips Laboratory, Hanscom AF Base, M. A., pp. 17-43.

Fujiwara, A., Kawaguchi, J., Yeomans, D. K., Abe, M., Mukai, T., Okada, T., Saito, J., Yano, H., Yoshikawa, M., Scheeres, D. J., Barnouin-Jha, O., Cheng, A. F., Demura, H., Gaskell, R. W., Hirata, N., Ikeda, H., Kominato, T., Miyamoto, H., Nakamura, A. M., Nakamura, R., Sasaki, S. and Uesugi, K. 2006. The rubble-pile asteroid Itokawa as observed by Hayabusa. Science 312, 1330-1334.

Green, S. F., Meadows, A. J. and Davies, J. K. 1985. Infrared observations of the extinct cometary candidate minor planet (3200) 1983TB. Mon. Not. Roy. Astron. Soc. 214, 29P-36P.

Harris, A. W. 1998. A Thermal Model for Near-Earth Asteroids. Icarus 131, 291-301.

Harris, A. W., Davies, J. K. and Green, S. F. 1998. Thermal infrared spectrophotometry of the near-Earth asteroids 2100 Ra-Shalom and 1991 EE. Icarus 135, 441-450.

Harris, A. W. and Davies, J. K. 1999. Physical Characteristics of near-Earth asteroids from thermal infrared spectrophotometry. Icarus 142, 464-475.

Harris, A. W. and Lagerros, J. S. V. 2002. Asteroids in the Thermal Infrared. In: W. F. Bottke, A. Cellino, P. Paolicchi and R. P. Binzel (Eds.), Asteroids III, The University of Arizona Press, Tucson, pp. 205-218.

Harris, A. W., Mueller, M., Delbò, M. and Bus, S. J. 2005. The surface properties of small asteroids: Peculiar Betulia - A case study. Icarus 179, 95-108.

Harris, A. W., Mueller, M., Delbó, M. and Bus, S. J. 2007. Physical Characterization of the Potentially-Hazardous High-Albedo Asteroid (33342) 1998 WT24 from Thermal-Infrared Observations. Icarus In press,

Ishiguro, M., Abe, M., Ohba, Y., Fujiwara, A., Fuse, T., Terada, H., Goto, M., Kobayashi, N., Tokunaga, A. T. and Hasegawa, S. 2003. Near-infrared observations of MUSES-C mission target. Publications of the Astronomical Society of Japan 55, 691-699.

Kaasalainen, M., Abe, M., Byron, J., Delbó, M., Di Martino, M., Higgins, D., Kitazato, K., Lowry, S., Masi, G., Mueller, M., Näränen, J., Vokrouhlický, D., Warner, B., Weissman, P. and Young, J., Photometric observations 2001–2004 and modelling of (25143) Itokawa. ASP Conference Series. , 2007, p. In press.

Konopliv, A. S., Miller, J. K., Owen, W. M., Yeomans, D. K. and Giorgini, J. D. 2002. A Global Solution for the Gravity Field, Rotation, Landmarks, and Ephemeris of Eros. Icarus 160, 289-299.

Lagerros, J. S. V. 1998. Thermal physics of asteroids IV. Thermal infrared beaming. Astron. Astrophys. 332, 1123-1132.

Lebofsky, L. A. and Rieke, G. H. 1979. Thermal properties of 433 Eros. Icarus 40, 297-308.

Lebofsky, L. A., Veeder, G. J., Rieke, G. H., Lebofsky, L. A., Matson, D. L., Kowal, C., Wynn-Williams, C. G. and Becklin, E. E. 1981. The Albedo and Diameter of 1862 Apollo. Icarus 48, 335-338.

Lebofsky, L. A., Sykes, M. V., Tedesco, E. F., Veeder, G. J., Matson, D. L., Brown, R. H., Gradie, J. C., Feierberg, M. A. and Rudy, R. J. 1986. A refined "standard" thermal model for asteroids based on observations of 1 Ceres and 2 Pallas. Icarus 68, 239-251.

Lebofsky, L. A. and Spencer, J. R. 1989. Radiometry and thermal modeling of asteroids. In: R. P. Binzel, T. Gehrels and M. S. Matthews (Eds.), Asteroids II, Univ. of Arizona Press, Tucson, pp. 128-147.

Li, J. Y., A'Hearn, M. F. and McFadden, L. A. 2004. Photometric analysis of Eros from NEAR data. Icarus 172, 415-431.

Lim, L. F., Emery, J. P. and McConnochie, T. H., Thermal Infrared (8-13 micron) Spectra of the NEA 2100 Ra-Shalom. DPS, 2005a, p. 629.

Lim, L. F., McConnochie, T. H., Bell, J. F. and Hayward, T. L. 2005b. Thermal infrared (8-13 μm) spectra of 29 asteroids: the Cornell Mid-infrared Asteroid Spectroscopy (MIDAS) Survey. Icarus 173, 385-408.

McFadden, L. A., Gaffey, M. J. and McCord, T. B. 1984. Mineralogical-petrological characterization of near-Earth asteroids. Icarus 59, 25-40.

Mitchell, D. L., Hudson, R. S., Ostro, S. J. and Rosema, K. D. 1998. Shape of asteroid 433 Eros from inversion of Goldstone radar doppler spectra. Icarus 131, 4-14.

Morrison, D., Gradie, J. C. and Rieke, G. H. 1976. Radiometric Diameter and Albedo of Remarkable Asteroid 1976aa. Nature 260, 691-691.

Mottola, S., Erikson, A., Harris, A. W., Hahn, G., Neukum, G., Buie, M. W., Sears, W. D., Harris, A. W., Tholen, D. J., Whiteley, R. J., Magnusson, P., Piironen, J., Kwiatkowski, T., Borczyk, W., Howell, E. S., Hicks, M. D., Fevig, R., Krugly, Y. N., Velichko, F. P., Chiorny, V. G., Gaftonyuk, N. M., Di Martino, M., Pravec, P., Šarounová, L., Wolf, M., Worman, W., Davies, J. K., Schober, H.-J. and Pych, W. 1997. Physical model of near-Earth asteroid 6489 Golevka (1991 JX) from optical and infrared observations. Astron. J. 114, 1234-1245.

Mueller, M., Harris, A. W., Delbo, M. and Bus, S. J., The Sizes and Albedos of Near-Earth Asteroids, Including 6489 Golevka, from Recent IRTF Observations. DPS Meeting 35, 2003, p. 955.

Mueller, M., Delbó, M., Di Martino, M., Harris, A. W., Kaasalainen, M. and Bus, S. J., Indications for regolith on Itokowa from thermal-infrared observations. ASP Conference Series. In press., 2007a, p.

Mueller, M., Harris, A. W. and Fitzsimmons, A. 2007b. Size, albedo, and taxonomic type of potential spacecraft target asteroid (10302) 1989 ML. Icarus 187, 611-615.

Müller, T. G. and Lagerros, J. S. V. 1998. Asteroids as far-infrared photometric standards for ISOPHOT. Astron. Astrophys. 338, 340-352.

Müller, T. G., Sterzik, M. F., Schutz, O., Pravec, P. and Siebenmorgen, R. 2004. Thermal infrared observations of near-Earth asteroid 2002 NY40. Astron. Astrophys. 424, 1075-1080.

Müller, T. G., Sekiguchi, T., Kaasalainen, M., Abe, M. and Hasegawa, S. 2005. Thermal infrared observations of the Hayabusa spacecraft target asteroid 25143 Itokawa. Astron. Astrophys. 443, 347-355.

Pravec, P., Šarounová, L. and Wolf, M. 1996. Lightcurves of 7 Near-Earth Asteroids. Icarus 124, 471-482.

Pravec, P., Scheirich, P., Kušnirák, P., Šarounová, L., Mottola, S., Hahn, G., Brown, P., Esquerdo, G., Naiser, N., Krzeminski, Z., Pray, D. P., Warner, B. D., Harris, A. W., Nolan, M. C., Howell, E. S., Benner, L. A. M., Margot, J.-L., Galád, A., Holliday, W., Hicks, M. D., Krugly, Y. N., Tholen, D., Whiteley, R., Marchis, F., DeGraff, D. R., Grauer, A., Larson, S., Velichko, F. P., Cooney Jr., W. R., Stephens, R., Zhu, J., Kirsch, K., Dyvig, R., Snyder, L., Reddy, V., Moore, S., Gajdoš, Š.,

Világi, J., Masi, G., Higgins, D., Funkhouser, G., Knight, B., Slivan, S., Behrend, R., Grenon, M., Burki, G., Roy, R., Demeautis, C., Matter, D., Waelchli, N., Revaz, Y., Klotz, A., Rieugné, M., Thierry, P., Cotrez, V., Brunetto, L. and Kober, G. 2006. Photometric survey of binary near-Earth asteroids. Icarus 181, 63-93.

Rieke, G. H., Lebofsky, M. J. and Low, F. J. 1985. An Absolute Photometric System at 10-Mu-M and 20-Mu-M. Astron. J. 90, 900-906.

Sekiguchi, T., Abe, M., Boehnhardt, H., Dermawan, B., Hainaut, O. R. and Hasegawa, S. 2003. Thermal observations of MUSES-C mission target (25143) 1998 SF36. Astron. Astrophys. 397, 325-328.

Stuart, J. S. and Binzel, R. P. 2004. Bias-corrected population, size distribution, and impact hazard for the near-Earth objects. Icarus 170, 295-311.

Sullivan, R. J., Thomas, P. C., Murchie, S. L. and Robinson, M. S. 2002. Asteroid Geology from Galileo and NEAR Shoemaker Data. In: W. F. Bottke, A. Cellino, P. Paolicchi and R. P. Binzel (Eds.), pp.

Tedesco, E. F. and Gradie, J. 1987. Discovery of M class objects among the near-Earth asteroid population. Astron. J. 93, 738-746.

Thomas, P. C., Joseph, J., Carcich, B., Veverka, J., Clark, B. E., Bell, J. F., Byrd, A. W., Chomko, R., Robinson, M., Murchie, S., Prockter, L., Cheng, A., Izenberg, N., Malin, M., Chapman, C., McFadden, L. A., Kirk, R., Gaffey, M. and Lucey, P. G. 2002. Eros: Shape, topography, and slope processes. Icarus 155, 18-37.

Tokunaga, A. T. 1984. A re-evaluation of the 20-μm magnitude system. Astron. J. 89, 172-175.

Veeder, G. J., Hanner, M. S., Matson, D. L., Tedesco, E. F., Lebofsky, L. A. and Tokunaga, A. T. 1989. Radiometry of near-Earth asteroids. Astron. J. 97, 1211-1219.

Veverka, J., Robinson, M., Thomas, P., Murchie, S., Bell III, J. F., Izenberg, N., Chapman, C., Harch, A., Bell, M., Carcich, B., Cheng, A., Clark, B., Domingue, D., Dunham, D., Farquhar, R., Gaffey, M. J., Hawkins, E., Joseph, J., Kirk, R., Li, H., Lucey, P., Malin, M., Martin, P., McFadden, L., Merline, W. J., Miller, J. K., Owen, W. M., Peterson, C., Prockter, L., Warren, J., Wellnitz, D., Williams, B. G. and Yeomans, D. K. 2000. NEAR at Eros: Imaging and Spectral Results. Science 289, 2088-2097.

Wisniewski, W. Z., Michalowski, T. M., Harris, A. W. and McMillan, R. S. 1997. Photometric observations of 125 asteroids. Icarus 126, 395-449.

Wolters, S. D., Green, S. F., McBride, N. and Davies, J. K. 2005. Optical and thermal infrared observations of six near-Earth asteroids in 2002. Icarus 175, 92-110.

Zappalà, V., Cellino, A., Barucci, M. A., Fulchignoni, M. and Lupishko, D. F. 1990. An analysis of the amplitude-phase relationship among asteroids. Astron. Astrophys. 231, 548-560.

Zellner, B. 1976. Physical properties of asteroid 433 Eros. Icarus 28, 149-153.

Tables

Table 1
Observational circumstances, instrument configuration and notes for asteroids observed at the JKT and UKIRT in 2002.

Asteroid	Date (UT)	Start –End (hh:mm UT)	Exp. time (s)	No. of frames	r (AU)	Δ (AU)	α°	Notes
JKT								
(433) Eros	28.1 Sep.	23:04 – 03:39	5.0	47	1.590	0.639	18.0	
	29.0 Sep.	20:37 – 03:22	5.0	76	1.588	0.640	18.6	
	30.0 Sep.	23:01 – 00:26	5.0	60	1.585	0.642	19.1	
(137032) 1998 UO_1	26.2 Sep.	03:00 – 06:10	120.0	43	1.201	0.337	47.2	
UKIRT								
(138258) 2000 GD_2	23.4 Mar.	09:50 – 11:40	N/A	N/A	1.084	0.101	28.0	Michelle in Imaging mode; 10.3, 12.5 and 18.5 μm filters used.
(433) Eros	28.4 Sep.	09:39 – 09:58	17.6	12	1.589	0.639	18.2	4 pixel slit width. Clear skies. Ratio star BS 8650 is a spectroscopic binary.
(66063) 1998 RO_1	29.4 Sep.	08:18 – 09:32	16.4	48	1.124	0.183	44.5	2 pixel slit width. Only object observed on 29 Sep. not also observed on another night. Observed after 2000 ED_{104} (sky clear) and before Eros (cirrus), so may be affected by cloud.
(137032) 1998 UO_1	28.5 Sep.	10:52 – 11:12	17.6	12	1.230	0.349	42.8	4 pixel slit width. Ratio star BS 915.

Notes. Exposure time is per frame. Ephemerides are taken from JPL Horizons. r, Δ, and α given for midpoint of observation.

Table 2
Flux-calibrated asteroid thermal IR fluxes observed in 2002 at UKIRT

(433) Eros, 2002-09-28			
Wavelength (μm)	**F_{ast} ($\times 10^{-13}$ W m^{-2} μm^{-1})**	**Standard error ($\times 10^{-13}$ W m^{-2} μm^{-1})**	**No. of Pixels[a]**
8.120	2.86	0.032	10
8.369	2.99	0.020	10
8.625	3.07	0.022	10
8.884	3.17	0.012	10
9.159	3.15	0.013	11
10.166	3.22	0.0097	12
10.476	3.19	0.0089	12
10.783	3.12	0.014	12
11.088	3.08	0.012	12
11.393	3.06	0.0066	12
11.700	3.05	0.010	12
12.011	2.99	0.011	12
12.329	2.84	0.021	12
(66063) 1998 RO_1, 2002-09-28			
Wavelength (μm)	**F_{ast} ($\times 10^{-15}$ W m^{-2} μm^{-1})**	**Standard error ($\times 10^{-15}$ W m^{-2} μm^{-1})**	**No. of pixels[a]**
8.641	1.52	0.020	51
10.421	1.78	0.022	32
11.249	2.44	0.021	32
12.081	2.18	0.023	32
2000 GD2, 2002-03-23			
Wavelength (μm)	**F_{ast} ($\times 10^{-15}$ W m^{-2} μm^{-1})**	**Standard error ($\times 10^{-15}$ W m^{-2} μm^{-1})**	
10.3	3.76	0.4	
12.5	3.70	0.4	
18.5	1.14	0.2	

Notes. [a] i.e. number of pixels over which flux is binned (spectroscopy mode only)

Table 3
Best-fit geometric albedos and effective diameters using the STM, FRM and NEATM.

Object /Date	**STM**		**FRM**		**NEATM Default η**			**NEATM Fitted/chosen η**					**Fig.**
	p_v	**D_{eff} (km)**	**p_v**	**D_{eff} (km)**	**η**	**p_v**	**D_{eff} (km)**	**η**	**p_v**	**D_{eff} (km)**	**H_V (mag)**	**α°**	
(433) Eros 2002-09-28	0.27	21.91	0.08	40.30	1.0	0.23	24.02	**0.95**	**0.24**	**23.31**	10.32	18	4
(66063) 1998 RO_1 2002-09-29	0.65	0.42	**0.30**	**0.62**	1.0	0.57	0.45		N/A		18.0	45	5
(137032) 1998 UO_1 2002-09-28					1.5	>0.29	<1.13				16.7	43	
(138258) 2000 GD_2 2002-03-23	0.49	0.29	0.24	0.41	1.0	0.45	0.30	**0.74**	**0.56**	**0.27**	19.11	28	6

Notes. Adopted values given in bold. Mean H_V of (138258) 2000 GD_2 from Minor Planet Center (http://cfa-www.harvard.edu/iau/mpc.html) uncertainty ± 0.5 mag. Mean H_V of (66063) 1998 RO_1 from Pravec *et al.* (2006), uncertainty < 0.1 mag. Uncertainty of p_v [with the exception of (138258) 2000 GD_2, see Section 4.4], D_{eff} and η is 30%, 15% and 20% respectively.

Table 4
Effective diameters D_{eff}, geometric albedos p_v, and beaming parameters η, for S- and Q-type NEAs, and NEAs with derived beaming parameters η.

Asteroid	Date obs. yyyy-mm-dd	Thermal IR Flux Source [a]	NEATM Fit Source (if different)	Tax. Type	α°	p_v	±	D_{eff}	±	η	±
(433) Eros	1975-01-17	Lebofsky and Rieke (1979)	Harris (1998)	S	9.9	0.20	0.06	[b] 23.6	3.5	1.05	0.23
	1998-06-27	Harris and Davies (1999)			30.9	0.21	0.06	[b] 23.6	3.5	1.07	0.22
	2002-09-22	Lim *et al.* (2005b)	This work.		15	0.31	0.09	20.2	3.0	0.81	0.16
	2002-09-28	This work.			18.2	0.24	0.07	[b] 23.3	3.5	0.95	0.19
	(average)					0.22	[c] 0.02	[b] 23.5	0.2	[d] 1.02	[c] 0.06
	(spacecraft)	p_v from Li *et al.* (2004); D_{eff} from a volume of 2535 ± 20 km^3 reported by Thomas *et al.* (2002).				0.23	0.02	16.92	0.04		
(1566) Icarus	1987-06-23	Veeder *et al.* (1989)	Harris (1998)	S	93	0.33	0.10	1.27	0.19	[e] (1.2)	
(1580) Betulia	2002-06-02	Harris *et al.* (2005)		C	53	0.11	0.03	3.82	0.57	1.09	0.22
(1620) Geographos	1983-03-11	Veeder *et al.* (1989)	Harris (1998)	S	34	0.26	0.08	2.5	0.4	(1.2)	
(1627) Ivar	1985-07-10	Veeder *et al.* (1989)	Harris (1998)	S	53	0.12	0.04	10.2	1.5	(1.2)	
	2000-03-06	lightcurve corrected values (Delbó, private communication, 2004)	Delbó *et al.* (2003)		5	0.15	0.05	9.12	1.37	(1.0)	
	(average)					0.14	0.04	9.66	1.45		
(1685) Toro	1981-03-12	Veeder *et al.* (1989)	Harris (1998)	S	18	0.29	0.09	4.1	0.6	(1.2)	
(1862) Apollo	1980-11-26	Lebofsky *et al.* (1981)	Harris (1998)	Q	35	0.26	0.08	1.45	0.22	1.15	0.23
(1866) Sisyphus	1985-07-11	Veeder *et al.* (1989)	Delbo (2004)	S	35	0.14	0.04	8.9	1.3	1.14	0.23
	2000-03-17	Delbó *et al.* (2003)			16	0.15	0.05	8.48	1.27	(1.0)	
	(average)					0.15	0.04	8.7	1.3		
(1915) Quetzalcoatl	1981-03-12	Veeder *et al.* (1989)	Harris (1998)	S	29	0.31	0.09	0.4	0.06	(1.2)	
(1980) Tezcatlipoca	1997-08-29	Harris and Davies (1999)		Sl	62.9	0.14	0.04	[f] 5.7	0.9	1.54	0.31
	1997-08-31	Harris and Davies (1999)			63.4	0.15	0.05	[f] 5.6	0.8	1.64	0.33
	(average)					0.15	0.04	5.6	0.8	1.59	0.32
(2062) Aten	1976-01-26	Morrison *et al.* (1976)	Harris (1998)	S	50	0.28	0.08	0.91	0.14	(1.2)	
(2100) Ra-Shalom	1997-08-31	Harris *et al.* (1998)		Xc	40.6	0.13	0.04	2.48	0.37	1.80	0.4
	2000-08-21	lightcurve corrected values (Delbó, private communication, 2004)	Delbó *et al.* (2003)		39	0.083	0.02	2.79	0.42	2.32	0.36
	2003-08-22	Lim *et al.* (2005a)	Thermophysical model derived D_{eff}		39	0.13	0.02	2.3	0.3		
	(average)					0.11	0.03	2.64	0.40	2.06	0.41
(3200) Phaethon	1984-12-20	Green *et al.* (1985)	Harris (1998)	B, F	48.3	0.11	0.03	5.1	0.8	1.6	0.3
(3554) Amun	1986-03-12	Tedesco and Gradie (1987)	Harris (1998)	M	16.4	0.17	0.05	2.1	0.3	1.2	0.2
(3671) Dionysus	1997-06-02	Harris and Davies (1999)	Delbo (2004)	Cb	57.7	0.16	0.05	1.5	0.2	3.1	0.6

Table 4 continued.

Asteroid	Date obs. yyyy-mm-dd	Thermal IR Flux Source [a]	NEATM Fit Source (if different)	Tax. Type	α°	p_v	±	D_{eff}	±	η	±
(5381) Sekhmet	2003-05-12	Delbo (2004)		V	42	0.25	0.08	1.3	0.2	1.5	0.2
	2003-05-13	Delbo (2004)			38	0.24	0.07	1.4	0.2	1.7	0.2
	2003-05-14	Delbo (2004)			33	0.30	0.09	1.2	0.2	1.3	0.1
	2003-05-15	Delbo (2004)			29	0.24	0.07	1.4	0.2	1.8	0.2
	2003-05-16	Delbo (2004)			24	0.22	0.07	1.4	0.2	1.9	0.3
	2003-06-02	Delbo (2004)			44	0.22	0.07	1.5	0.2	1.9	0.8
	(average)					0.25	0.08	1.4	0.2	1.7	0.3
(5587) 1990 SB	2001-04-08	Delbo (2004)		Sq	19	0.25	0.08	4.0	0.60	1.1	0.1
	2001-05-10	Delbó *et al.* (2003)			42	0.32	0.10	3.57	0.54	[g] 0.84	0.2
	(average)					0.29	0.09	3.8	0.57	0.97	0.19
(6455) 1992 HE	2002-03-22	Wolters (2005)	Wolters *et al.* (2005)	S	22	0.29	0.09	3.37	0.51	0.80	0.16
	2002-09-28	Wolters (2005)	Wolters *et al.* (2005)		31	0.24	0.07	3.55	0.53	0.79	0.16
	2002-09-30	Wolters (2005)	Wolters *et al.* (2005)		28	0.27	0.08	3.43	0.51	0.57	0.11
	(average)					0.27	0.08	3.45	0.52	0.72	0.14
(6489) Golevka	1995-06-16	Mottola *et al.* (1997)	Harris (1998)	S	88.8	0.63	0.19	0.29	0.04	[h] (1.2)	
	2003-05-15	Delbo (2004)	Mueller *et al.* (2003)		43	0.39	0.12	0.33	0.05	(1.0)	
(9856) 1991 EE	1991-09-11	Harris *et al.* (1998)		S	36	0.30	0.09	1.01	0.15	1.15	0.23
(10302) 1989 ML	2006-06-02	Mueller *et al.* (2007b)		E	52.3	0.37	0.11	0.276	0.041	2.48	0.49
(14402) 1991 DB	2000-03-16	Delbó *et al.* (2003)		C	36	0.14	0.04	0.6	0.09	1.04	0.1
(16834) 1997 WU_{22}	2000-08-21	Delbó *et al.* (2003)	Delbo (2004) [i]	S	59	0.30	0.09	2.0	0.30	(1.5)	
(19356) 1997 GH_3	2001-04-08	Delbo (2004)		S	31	0.29	0.09	1.0	0.15	(1.0)	
	2001-05-11	Delbó *et al.* (2003)			5	0.34	0.10	0.91	0.14	0.98	0.1
	(average)					0.32	0.10	1.0	0.15		
(25143) Itokawa	2001-03-11	Ishiguro *et al.* (2003)	Used Free Beaming parameter Model	S	24.3	0.35	0.11	0.30	0.05		
	2001-03-14	Sekiguchi *et al.* (2003)			27.5	0.23	0.07	0.35	0.05		
	2001-04-08	Delbo (2004)			108	0.19	0.06	0.37	0.06	(1.2)	
	2004-07-01	Müller *et al.* (2005)	Only Thermophysical Model (TPM) reported		24-108	0.19	$^{+0.11}_{-0.03}$	0.32	0.03	(1.5)	
	2001-07-10	Mueller *et al.* (2007a)	Only TPM reported		29	Not reported		0.28	0.04		
	(average)					0.24	0.07	0.32	0.05		
	(spacecraft)	D_{eff} from a volume of $(1.84 \pm 0.092) \times 10^7$ m^3 reported in Fujiwara *et al.* (2006); p_v calculated applying $H_V = 19.52$ (Kaasalainen *et al.*, 2007) in Eq. 1				0.26	0.04	0.328	0.006		

Table 4 continued.

Asteroid	Date obs. yyyy-mm-dd	Thermal IR Flux Source [a]	NEATM Fit Source (if different)	Tax. Type	α°	p_v	±	D_{eff}	±	η	±
(25330) 1999 KV_4	2001-05-10	Delbó *et al.* (2003)		B	54	0.052	0.02	3.21	0.48	1.5	0.2
	2003-05-14	Delbo (2004)			3	0.09	0.03	2.55	0.38	1.06	0.17
	2003-06-02	Delbo (2004)			16	0.08	0.02	2.7	0.4	1.3	0.3
	(average)					0.07	0.02	2.82	0.42	1.29	0.26
(33342) 1998 WT_{24}	2001-12-04	Harris *et al.* (2007)		E	60.4	0.43	0.13	0.40	0.06	1.86	0.4
	2001-12-18	Harris *et al.* (2007)			67.5	0.75	0.23	0.31	0.05	0.61	0.12
	2001-12-19	Harris *et al.* (2007)			79.3	0.42	0.13	0.41	0.06	1.25	0.16
	2001-12-21	Harris *et al.* (2007)			93.4	0.18	0.05	0.62	0.09	2.7	0.1
	(average)					0.45	0.14	0.45	0.07	1.52	0.30
(35396) 1997 XF_{11}	2002-11-03	Delbo (2004)		E	63	0.18	0.05	1.18	0.18	1.8	0.2
	2002-11-05	Delbo (2004)			53	0.31	0.09	0.91	0.14	1.2	0.1
	2002-11-28	Delbo (2004)			30	0.32	0.10	0.89	0.13	1.3	0.8
	(average)					0.27	0.08	0.99	0.15	1.43	0.29
(53789) 2000 ED_{104}	2002-09-29	Wolters (2005)	Wolters *et al.* (2005)		60	0.18	0.05	1.18	0.18	1.80	0.36
	2002-09-30	Wolters (2005)	Wolters *et al.* (2005)		60	0.17	0.05	1.23	0.18	1.57	0.31
	(average)					0.18	0.05	1.21	0.18	1.69	0.34
(85953) 1999 FK_{21}	2002-02-21	Delbó *et al.* (2003)		S	35	0.32	0.10	0.59	0.09	0.91	0.4
(86039) 1999 NC_{43}	2000-03-17	Delbó *et al.* (2003)		Q	59	0.14	0.04	2.22	0.33	2.86	0.5
(108519) 2001 LF	2003-06-03	Delbo (2004)		C	45	0.05	0.02	2.0	0.3	1.4	0.1
(137170) 1999 HF_1	2002-03-22	Wolters (2005)	Wolters *et al.* (2005)	X	91	0.18	0.05	3.73	0.56	1.67	0.33
(138258) 2000 GD_2	2002-03-23	This work.		Sq	28	0.56	0.17	0.27	0.04	0.74	0.15
(139056) 2001 FY	2001-05-12	Delbó *et al.* (2003)		S	22	0.52	0.16	0.32	0.05	(1.0)	
(141593) 2002 HK_{12}	2002-09-28	Wolters (2005)	Wolters *et al.* (2005)		33	0.24	0.07	0.80	0.12	2.75	0.55
(142040) 2002 QE_{15}	2002-09-28	Wolters (2005)	Wolters *et al.* (2005)	A	62	0.15	0.05	1.94	0.29	1.53	0.77
2000 BG_{19}	2000-03-17	Delbó *et al.* (2003)		P	17	0.043	0.01	1.77	0.27	0.74	0.2
2000 EV_{70}	2000-03-17	Delbo (2004)		Q	14	0.60	0.18	0.15	0.02	(1.0)	
2002 BM_{26}	2002-02-21	Delbó *et al.* (2003)		P	60	0.023	0.01	0.84	0.13	3.1	0.4
2002 CT_{46}	2002-02-21	Delbó *et al.* (2003)		Sr	23	0.32	0.10	0.16	0.02	(1.0)	
2002 NX_{18}	2002-09-27	Wolters (2005)	Wolters *et al.* (2005)		52	0.034	0.01	2.13	0.32	1.18	0.24
	2002-09-30	Wolters (2005)	Wolters *et al.* (2005)		54	0.028	0.01	2.37	0.36	1.16	0.23
	(average)					0.031	0.01	2.25	0.34	1.17	0.23
2002 NY_{40}	2002-08-17	Müller *et al.* (2004)		Q	59	0.34	$^{+0.06}_{-0.05}$	0.27	0.01	(1.5)	

Table 4:

Notes. Uncertainties in p_v, D_{eff}, η are 30%, 15% and 20% unless given differently in the literature

[a] Unless otherwise indicated.

[b] At lightcurve maximum.

[c] Standard deviation.

[d] The average η-values are used in Fig. 10 (b)-(g), where 20% uncertainty is assumed, except for (433) Eros where the standard deviation of the measured η-values is adopted.

[e] η-values in brackets are default values used.

[f] D_{eff} in Harris and Davies (1999) given for lightcurve maximum. Recalculated for mean visual absolute magnitude using Eq. 1 given derived p_v and using H_v = 13.96 (Wisniewski *et al.*, 1997).

[g] Used η-value from Delbo (2004) rather than value given in Delbó *et al.* (2003).

[h] η-value inappropriate for phase angle of observation, result disregarded in analyses [as did Delbo (2004)].

[i] Delbó *et al.* (2003) have p_v = 0.22, D_{eff} = 1.87 km from same observations

Figures

Fig. 1

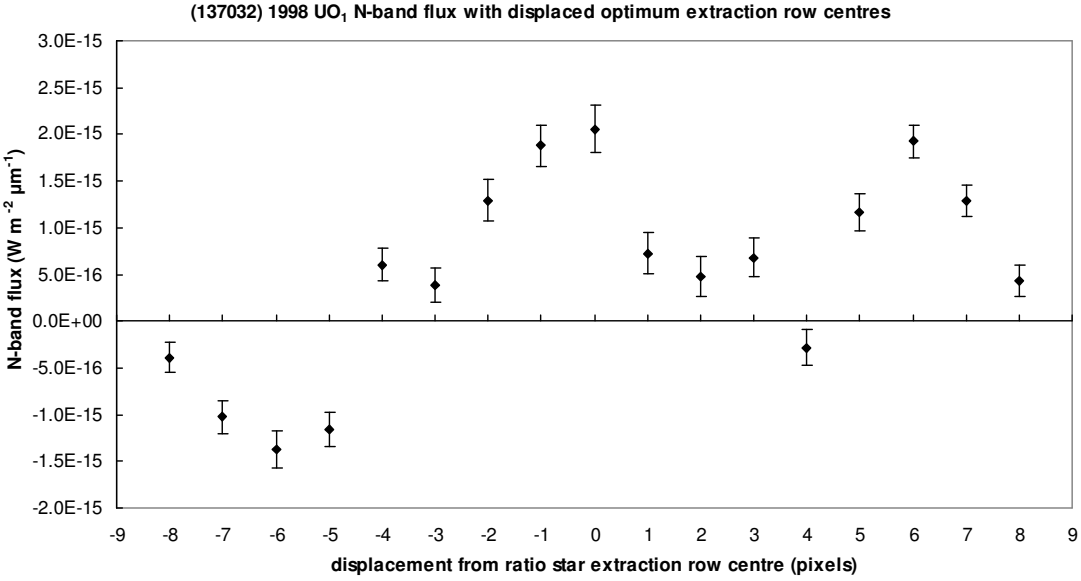

Fig. 2

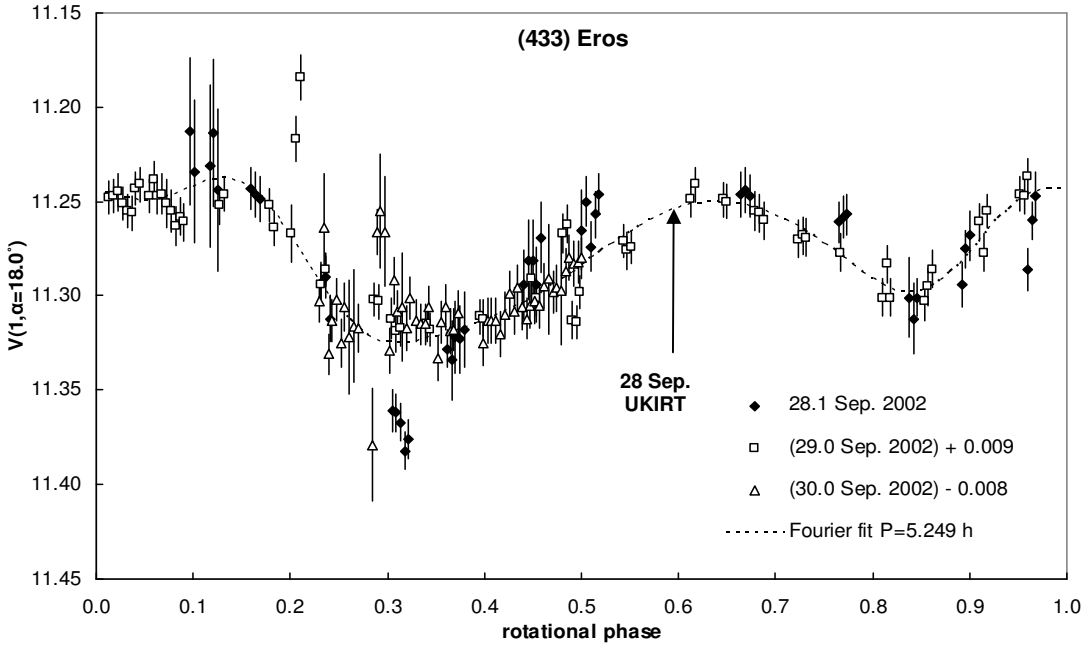
(433) Eros
V(1,α=18.0°)
rotational phase
28 Sep.
UKIRT
28.1 Sep. 2002
(29.0 Sep. 2002) + 0.009
(30.0 Sep. 2002) - 0.008
Fourier fit P=5.249 h
11.15
11.20
11.25
11.30
11.35
11.40
11.45
0.0
0.1
0.2
0.3
0.4
0.5
0.6
0.7
0.8
0.9
1.0

Fig. 3

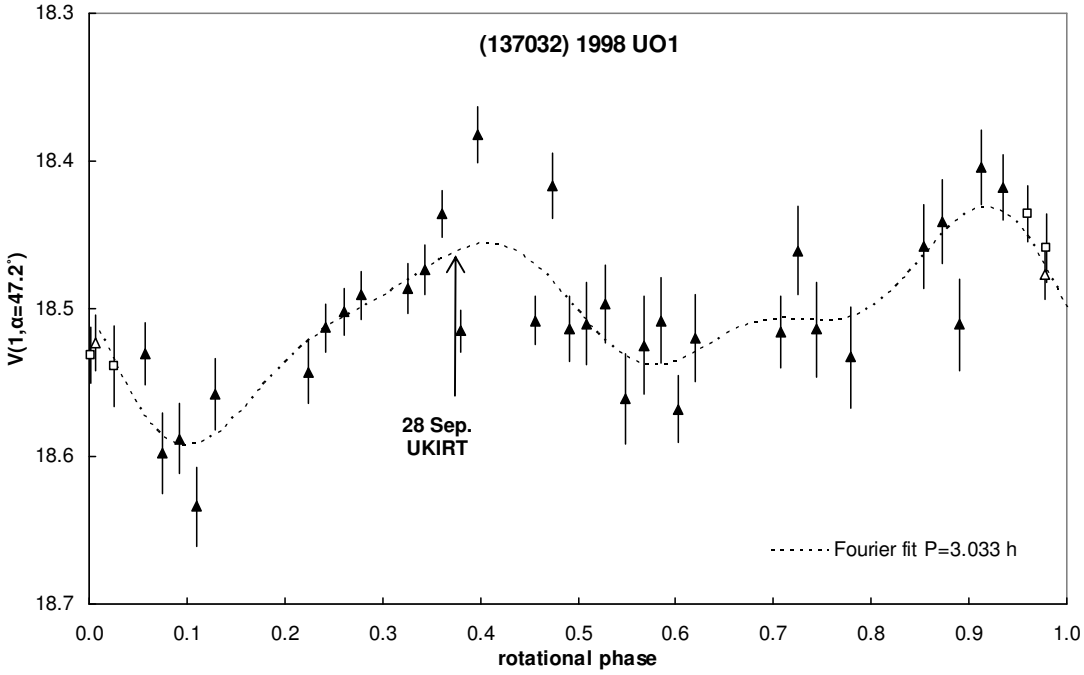
(137032) 1998 UO1
V(1,α=47.2°)
18.3
18.4
18.5
18.6
18.7
0.0
0.1
0.2
0.3
0.4
0.5
0.6
0.7
0.8
0.9
1.0
rotational phase
28 Sep.
UKIRT
Fourier fit P=3.033 h

Fig. 4

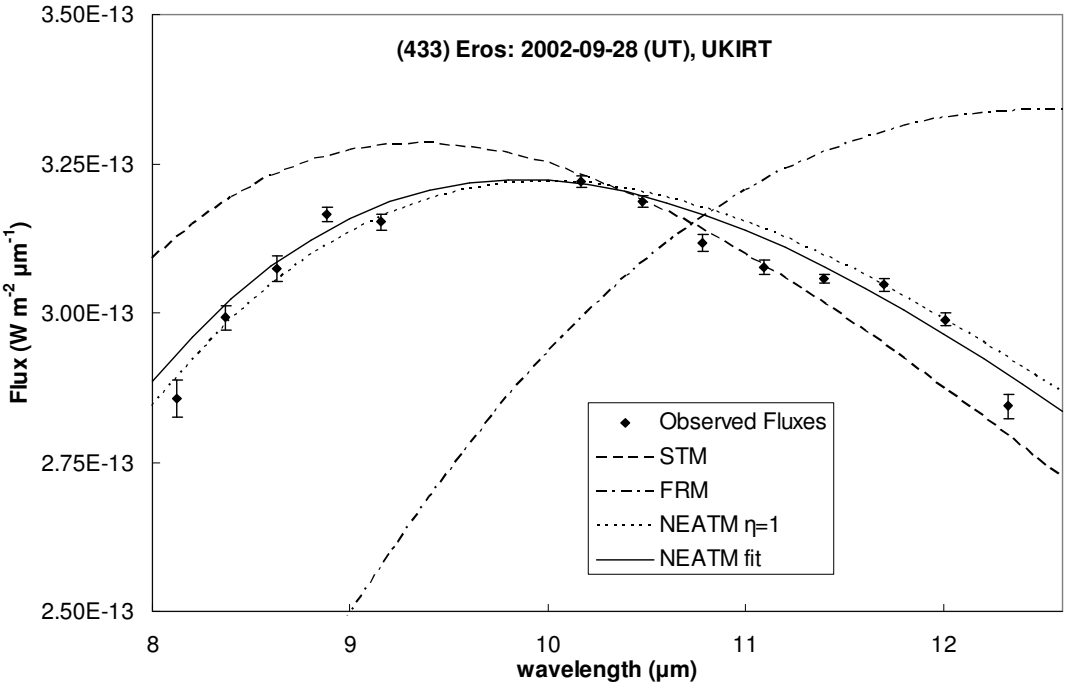
(433) Eros: 2002-09-28 (UT), UKIRT
3.50E-13
3.25E-13
3.00E-13
2.75E-13
2.50E-13
Flux (W m-2 µm-1)
8
9
10
11
12
wavelength (µm)
Observed Fluxes
STM
FRM
NEATM η=1
NEATM fit

Fig. 5

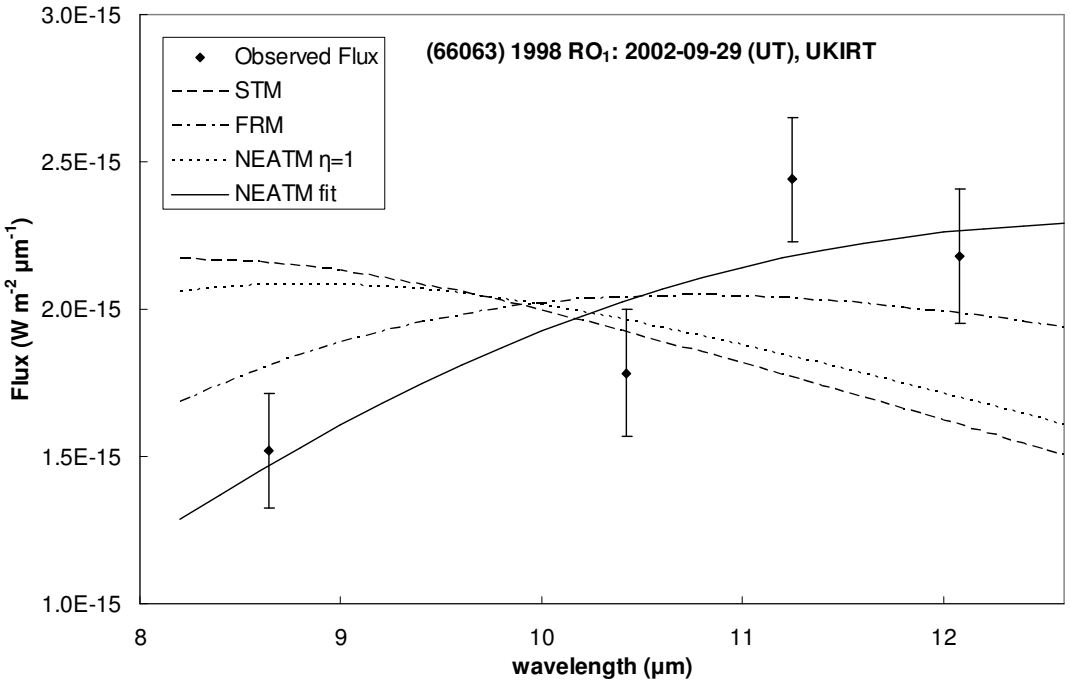
(66063) 1998 RO1: 2002-09-29 (UT), UKIRT
Observed Flux
STM
FRM
NEATM η=1
NEATM fit
Flux (W m-2 μm-1)
wavelength (μm)
3.0E-15
2.5E-15
2.0E-15
1.5E-15
1.0E-15
8
9
10
11
12

Fig. 6

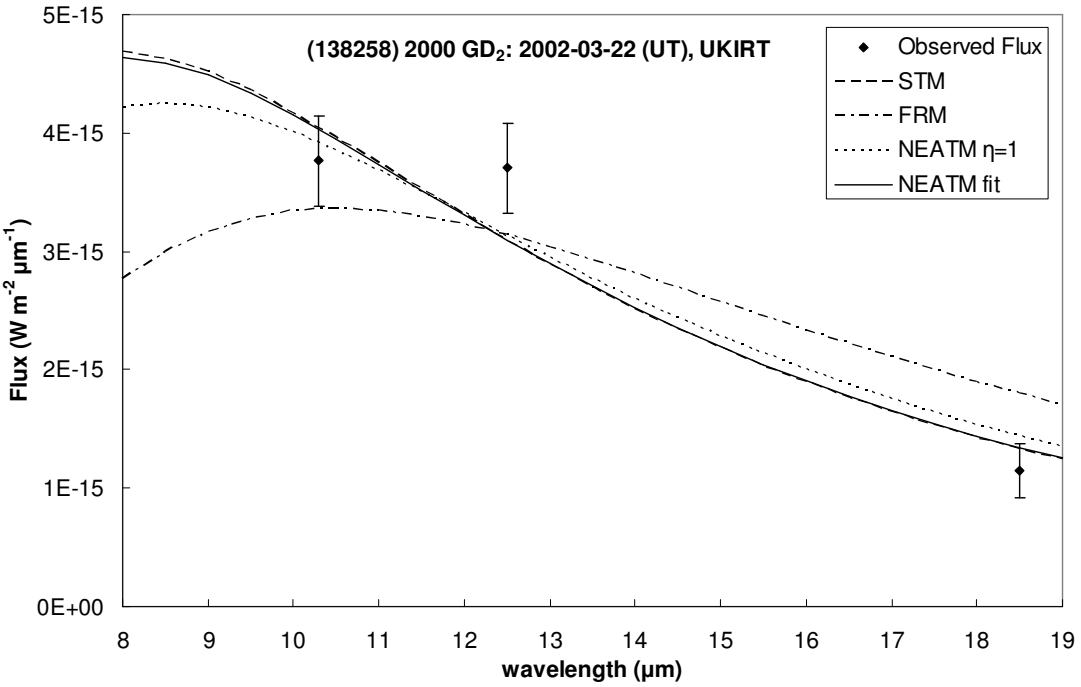
(138258) 2000 GD2: 2002-03-22 (UT), UKIRT
Observed Flux
STM
FRM
NEATM η=1
NEATM fit
Flux (W m-2 μm-1)
wavelength (μm)
5E-15
4E-15
3E-15
2E-15
1E-15
0E+00
8
9
10
11
12
13
14
15
16
17
18
19

Fig. 7

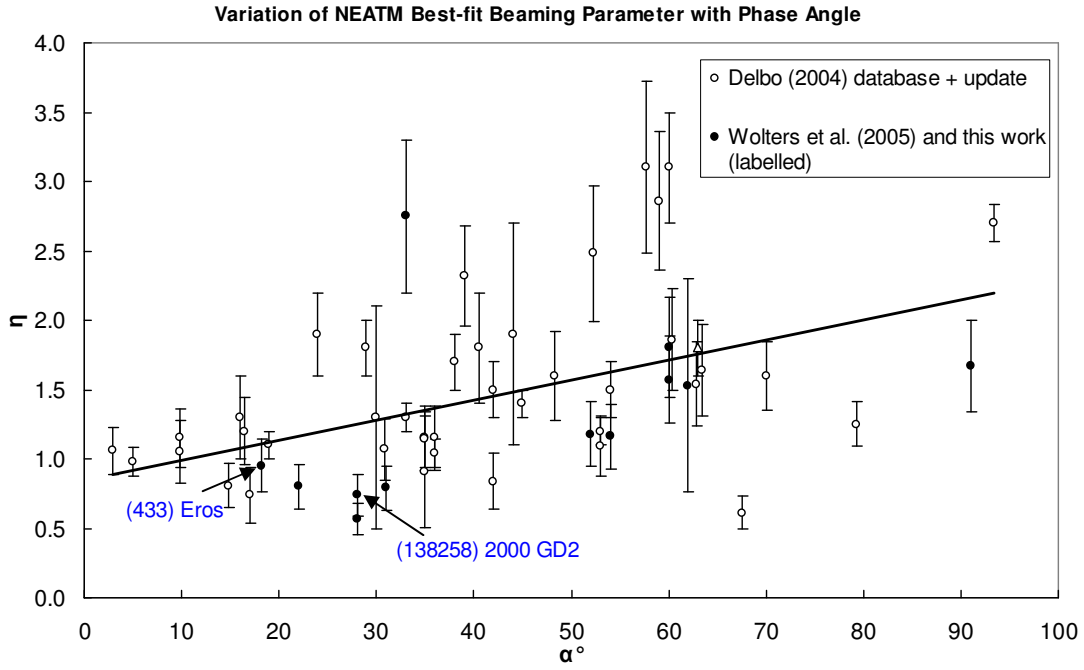
Variation of NEATM Best-fit Beaming Parameter with Phase Angle
Delbo (2004) database + update
Wolters et al. (2005) and this work (labelled)
(433) Eros
(138258) 2000 GD2
η
α°
0.0
0.5
1.0
1.5
2.0
2.5
3.0
3.5
4.0
0
10
20
30
40
50
60
70
80
90
100

Fig. 8

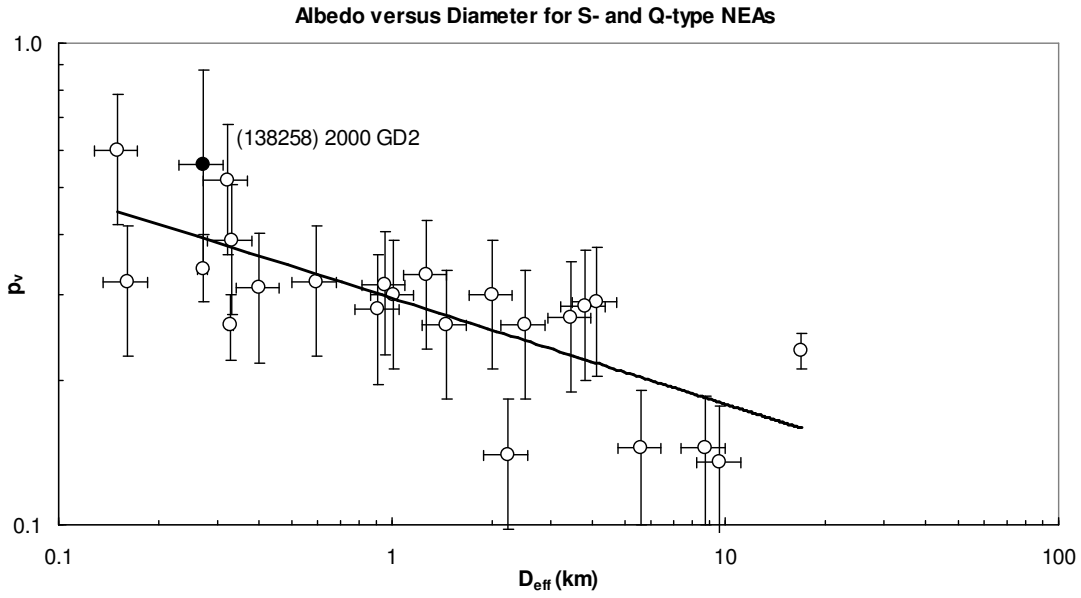
Albedo versus Diameter for S- and Q-type NEAs
1.0
0.1
(138258) 2000 GD2
p_v
0.1
1
10
100
D_{eff} (km)

Fig. 9

(a)

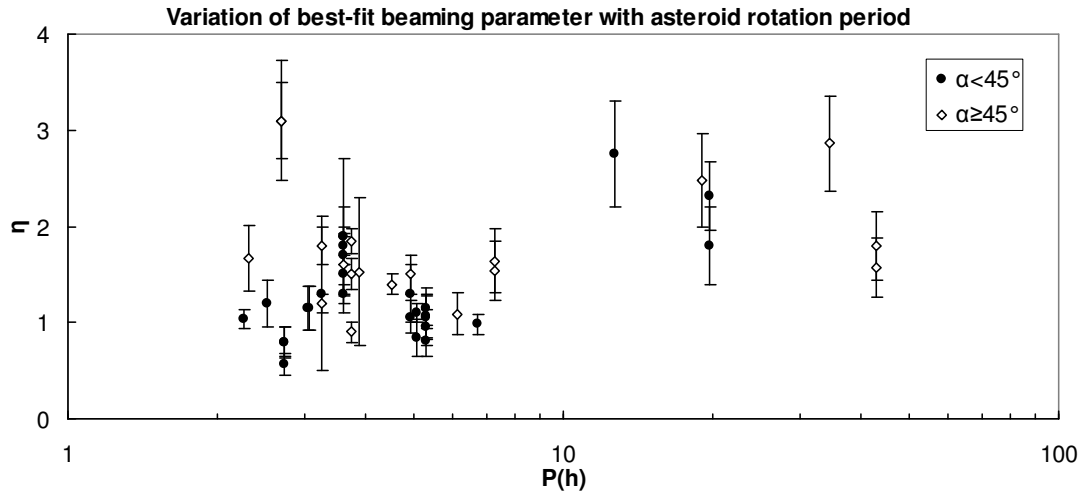
Variation of best-fit beaming parameter with asteroid rotation period
α<45°
α≥45°
η
P(h)
0
1
2
3
4
1
10
100

(b)

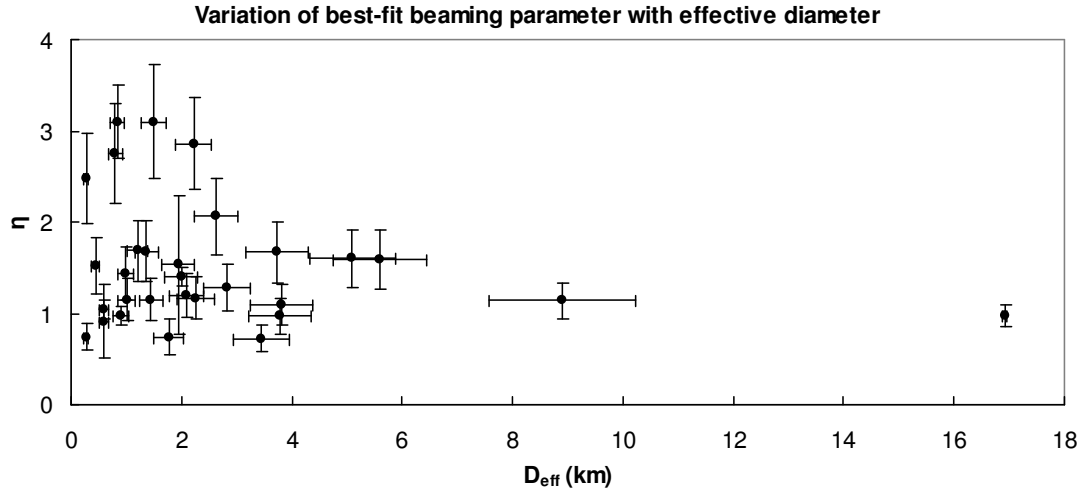
Variation of best-fit beaming parameter with effective diameter
η
D_eff (km)
0
1
2
3
4
0
2
4
6
8
10
12
14
16
18

(c)

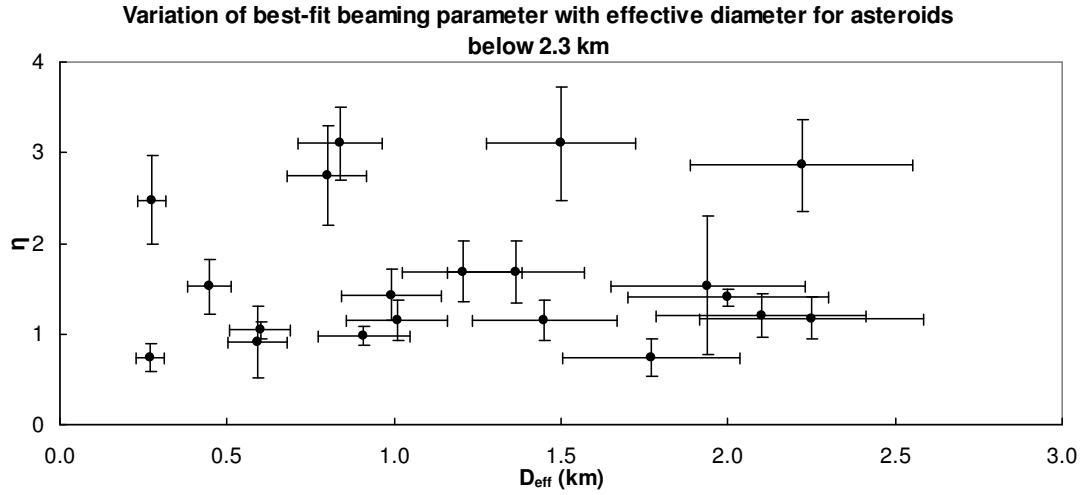
Variation of best-fit beaming parameter with effective diameter for asteroids below 2.3 km
η
D_eff (km)
0
1
2
3
4
0.0
0.5
1.0
1.5
2.0
2.5
3.0

(d)

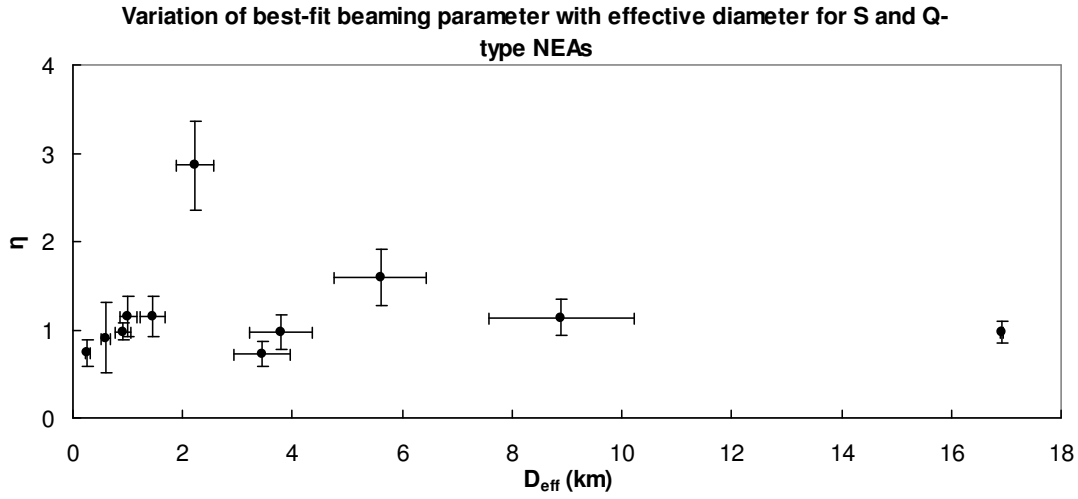
Variation of best-fit beaming parameter with effective diameter for S and Q-type NEAs
η
D_eff (km)
0
1
2
3
4
0
2
4
6
8
10
12
14
16
18

(e)

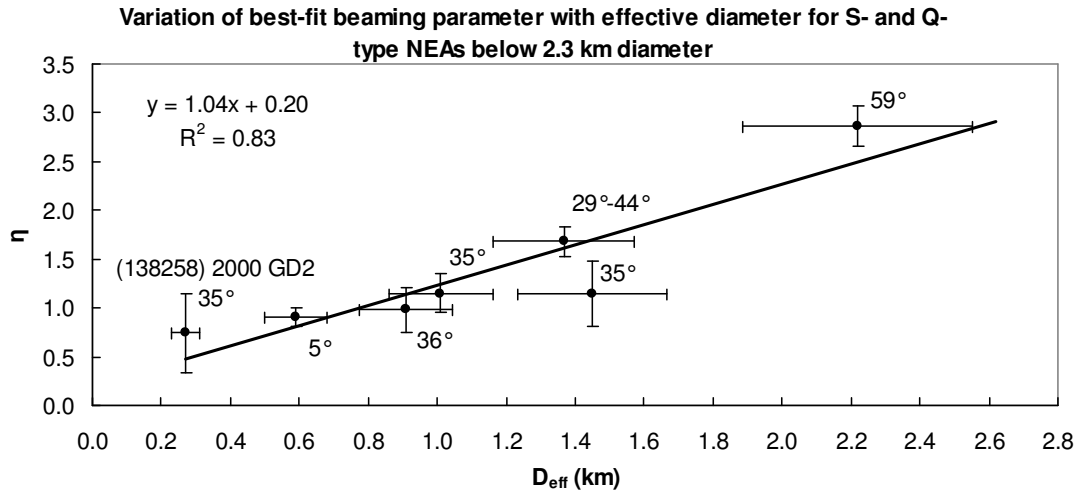
Variation of best-fit beaming parameter with effective diameter for S- and Q-type NEAs below 2.3 km diameter
y = 1.04x + 0.20
R2 = 0.83
(138258) 2000 GD2
35°
5°
36°
35°
35°
29°-44°
59°
η
D_eff (km)
0.0
0.5
1.0
1.5
2.0
2.5
3.0
3.5
0.0
0.2
0.4
0.6
0.8
1.0
1.2
1.4
1.6
1.8
2.0
2.2
2.4
2.6
2.8

(f)

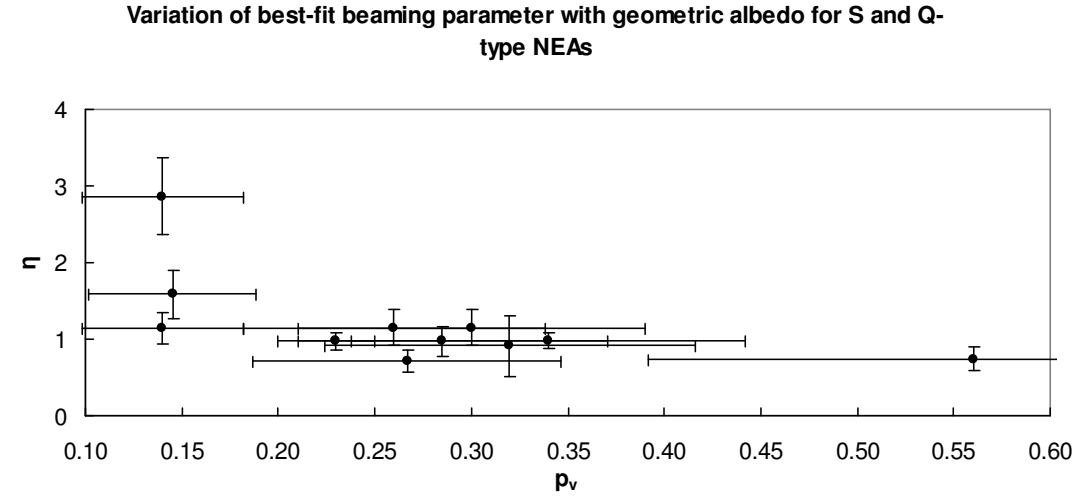
Variation of best-fit beaming parameter with geometric albedo for S and Q-type NEAs
η
p_v
0
1
2
3
4
0.10
0.15
0.20
0.25
0.30
0.35
0.40
0.45
0.50
0.55
0.60

(g)

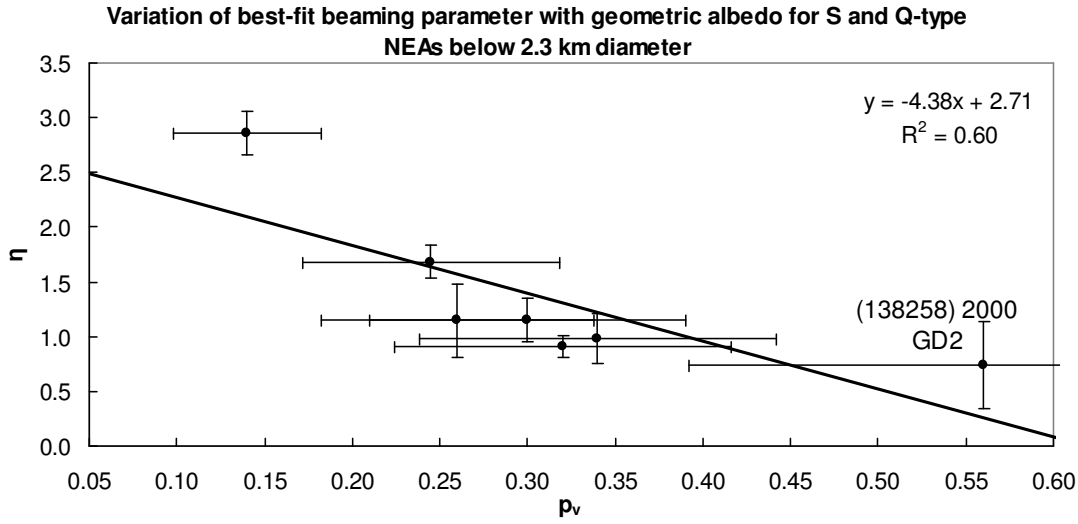
Variation of best-fit beaming parameter with geometric albedo for S and Q-type NEAs below 2.3 km diameter
y = -4.38x + 2.71
R2 = 0.60
(138258) 2000 GD2
η
pv
3.5
3.0
2.5
2.0
1.5
1.0
0.5
0.0
0.05
0.10
0.15
0.20
0.25
0.30
0.35
0.40
0.45
0.50
0.55
0.60

Figure Captions

Fig. 1. N-band flux of asteroid (137032) 1998 UO_1 with different optimum extraction row centres, displaced from the row centres used to extract the ratio star (BS 915) spectrum. The amplitude gives an indication of the electronic pickup noise.

Fig. 2. Composite lightcurve of (433) Eros combining JKT observations on 28.1, 29.0 and 30.0 Sep. 2002, using a 6th order Fourier fit P = 5.249 ± 0.001 h. Mean magnitudes adjusted to that of 28.1 Sep. 2002, $\overline{V}(\alpha = 18.0°)$ = 11.28 ± 0.06 mag. t_0 = 0h 25 Sep. 2002 UT. The rotational phase of the midpoint of the UKIRT observation is shown.

Fig. 3. A 4th order Fourier fit to (137032) 1998 UO_1 JKT 26.2 September 2002 observations, P = 3.033 ± 0.006 h. t_0 = 0h, 25 September 2002., mean reduced magnitude $\overline{V}(\alpha)$ = 18.506 ± 0.006 (black triangles). White triangles were taken at the beginning of the observation and fold with the white squares taken at the end. The rotational phase of the midpoint of the UKIRT observation is shown.

Fig. 4. Standard Thermal Model (STM), Fast Rotating Model (FRM), and Near Earth Asteroid Thermal Model (NEATM) fits to spectrum of (433) Eros using Michelle lowN grating.

Fig. 5. Standard Thermal Model (STM), Fast Rotating Model (FRM), and Near Earth Asteroid Thermal Model (NEATM) fits to spectrum of (66063) 1998 RO_1 using Michelle lowN grating.

Fig. 6. Standard Thermal Model (STM), Fast Rotating Model (FRM), and Near Earth Asteroid Thermal Model (NEATM) fits to spectrum of (138258) 2000 GD_2 using Michelle in imaging mode.

Fig. 7. The relationship between phase angle (α) and fitted beaming parameters (η). (Open circles) are from the Delbo (2004) database [with updated values for (33342) 1998 WT_{24} and (1580) Betulia as indicated in Table 4] ; (filled circles) are from Wolters et al. (2005) and this work (labelled). The line shows a linear fit including all objects: η = (0.013 ± 0.004)α + (0.91 ± 0.17). Delbó (2004) found a linear fit η = (0.011 ± 0.002)α + (0.92 ± 0.07), therefore our updated trend is consistent. This trend could be used to derive a default η for a given α. The scatter of η is partly due to variation of the asteroids' thermal inertia, rotation period, spin axis and shape, but also due to the evening/morning effect. The triangular points are those marked as anomalous by Delbó et al. (2003) and Wolters et al. (2005).

Fig. 8. Geometric visible albedo versus effective diameter derived using NEATM for S- and Q-type NEAs.

Fig. 9. (a) Variation of NEATM best-fit beaming parameter η with: (a) rotation period P(h); (b) effective diameter D_{eff} (km); (c) effective diameter below 2.3 km (no trend found even if possibly anomalous points above η = 2 are excluded); (d) effective diameter for S- and Q-type asteroids only; (e) effective diameter for S- and Q-type asteroids below 2.3 km with data labels showing phase angle; (f) geometric albedo for S- and Q-type asteroids only; (g) geometric albedo for S- and Q-type asteroids below 2.3 km diameter. In (b)-(g) objects for which there is more than one observation have their values averaged (see Table 4).